



HAL
open science

Hybrid sampling/spectral method for solving stochastic coupled problems

Maarten Arnst, Christian Soize, Roger Ghanem

► **To cite this version:**

Maarten Arnst, Christian Soize, Roger Ghanem. Hybrid sampling/spectral method for solving stochastic coupled problems. *SIAM/ASA Journal on Uncertainty Quantification*, 2013, 1 (1), pp.218-243. 10.1137/120894403 . hal-00829060

HAL Id: hal-00829060

<https://hal.science/hal-00829060>

Submitted on 1 Jun 2013

HAL is a multi-disciplinary open access archive for the deposit and dissemination of scientific research documents, whether they are published or not. The documents may come from teaching and research institutions in France or abroad, or from public or private research centers.

L'archive ouverte pluridisciplinaire **HAL**, est destinée au dépôt et à la diffusion de documents scientifiques de niveau recherche, publiés ou non, émanant des établissements d'enseignement et de recherche français ou étrangers, des laboratoires publics ou privés.

HYBRID SAMPLING/SPECTRAL METHOD FOR SOLVING STOCHASTIC COUPLED PROBLEMS*

M. ARNST[†], C. SOIZE[‡], AND R. GHANEM[§]

Abstract. In this paper, we present a hybrid method that combines Monte Carlo sampling and spectral methods for solving stochastic coupled problems. After partitioning the stochastic coupled problem into subsidiary subproblems, the proposed hybrid method entails iterating between these subproblems in a way that enables the use of the Monte Carlo sampling method for subproblems that depend on a very large number of uncertain parameters and the use of spectral methods for subproblems that depend on only a small or moderate number of uncertain parameters. To facilitate communication between the subproblems, the proposed hybrid method shares between the subproblems a reference representation of all the solution random variables in the form of an ensemble of samples; for each subproblem solved by a spectral method, it uses a dimension-reduction technique to transform this reference representation into a subproblem-specific reduced-dimensional representation to facilitate a computationally efficient solution in a reduced-dimensional space. After laying out the theoretical framework, we provide an example relevant to microelectomechanical systems.

Key words. coupled problems, multiphysics, hybrid method, Monte Carlo, polynomial chaos

AMS subject classifications. 60H15, 60H25, 60H35, 65C05, 65C30, 65C50

1. Introduction. Coupled problems with various combinations of multiple physics, scales, and domains are found in numerous areas of science and engineering: Multiphysics models can take the form of a single equation that tightly couples different types of physical behavior, or they can take the form of a system of equations wherein the solution to certain equations is passed to other equations to determine physical properties or loadings or both. Multiscale models couple different types of behavior with fundamentally different descriptions at different scales. In multidomain models, physical behavior in different regions of space is coupled through a shared interface.

Partitioned methods are widely used for solving coupled problems. These methods most often split a coupled problem into subproblems that represent single-physics, single-scale, or single-domain behavior, and they then seek a global solution by iterating between subproblem solutions. The attraction of partitioned methods is that many coupled problems afford a natural decomposition into subproblems for which computational expertise and dedicated solvers already exist: partitioned methods enable immediate reuse of legacy solvers that are already available to solve subproblems.

The quantification of the effects of modeling errors and parametric uncertainties is always required to justify predictive capabilities of scientific and engineering models. A probabilistic framework is most often adopted, wherein uncertainties are propagated from uncertain input parameters to predictions using either the Monte Carlo sampling method [13] or spectral methods [7, 11, 19]. Within the current state of the art, the effectiveness of the Monte Carlo sampling and spectral methods is essentially as follows. On the one hand, the Monte Carlo sampling method is most computation-

*Part of this work was completed while M. Arnst was visiting the Université Paris-Est. This visit was supported by the Fonds de la Recherche Scientifique (FNRS) through a travel grant. Further, this work was supported by the Université de Liège through a starting grant.

[†]Université de Liège, Département Aérospatiale et Mécanique, Chemin des Chevreuils 1, B-4000 Liège, Belgium (maarten.arnst@ulg.ac.be).

[‡]Université Paris-Est, Laboratoire Modélisation et Simulation Multi Echelle, MSME UMR 8208 CNRS, 5 bd Descartes, 77454 Marne-la-Valle, France.

[§]University of Southern California, Department of Civil and Environmental Engineering, 3620 S Vermont Ave, Los Angeles, CA 90089, USA.

ally efficient for problems of “very high dimension,” that is, for problems that require a very large number of random variables to accurately characterize their uncertain features. On the other hand, spectral methods are indicated most for sufficiently smooth problems of “low or moderate dimension,” that is, for problems for which a small or moderate number of random variables suffices to accurately characterize the uncertain features, as well as for problems that admit adaptation relative to dimensionality [1, 2]. We emphasize that the merits and limitations of the Monte Carlo sampling and spectral methods depend on the problem and implementation specificities; further, much ongoing research is involved with extending the computational efficiency of spectral methods to problems of higher and higher dimension [5, 6].

In this paper, we consider partitioned methods for solving stochastic coupled problems. We focus on stochastic coupled problems that, when split into subproblems, yield one or more subproblems that require a very large number of random variables to accurately characterize their uncertain features, as well as one or more subproblems for which a small or moderate number of random variables suffices. For such stochastic coupled problems, we present a hybrid Monte Carlo sampling/spectral method. The proposed hybrid method seeks a global solution by iterating between the subproblems in a way that enables the use of the Monte Carlo sampling method for the subproblems of “very high dimension” and the use of spectral methods for the subproblems of “low or moderate dimension,” thus maximizing computational efficiency. To facilitate communication between the subproblems, the proposed hybrid method shares between the subproblems a reference representation of all the solution random variables in the form of an ensemble of samples; for each subproblem solved by a spectral method, it uses a dimension-reduction technique [1, 2] to transform this reference representation into a subproblem-specific reduced-dimensional representation to facilitate a computationally efficient solution in a reduced-dimensional space.

A typical example wherein the proposed hybrid method can be of use is a multi-physics parameter-passing problem wherein one subproblem has the form of a stochastic elliptic partial differential equation whose random coefficients oscillate very rapidly as a function of the position and that exhibits some homogenization owing to spatial averaging. Because many random variables can be expected to be required to accurately characterize these very rapidly oscillating coefficients, this subproblem can be expected to be of “very high dimension.” However, because only a small or moderate number of random variables can be expected to suffice to accurately characterize the homogenized solution, subproblems to which this solution is passed to determine their physical properties or loadings or both can be of “low or moderate dimension.”

The remainder of this paper is organized as follows. First, in Sec. 2, we present the proposed hybrid method. Next, in Sec. 3, we provide details on the implementation. Finally, in Secs. 4 and 5, we provide an illustration problem with numerical results.

2. Hybrid Monte Carlo sampling/spectral method.

2.1. Model problem. This paper is devoted to the determination of the solution to a stochastic coupled problem of the following form:

$$\begin{aligned} \mathbf{f}(\mathbf{U}, \mathbf{X}, \boldsymbol{\xi}) &= \mathbf{0}, & \mathbf{Y} &= \mathbf{h}(\mathbf{U}, \mathbf{X}, \boldsymbol{\xi}); \\ \mathbf{g}(\mathbf{Y}, \mathbf{V}, \boldsymbol{\zeta}) &= \mathbf{0}, & \mathbf{X} &= \mathbf{k}(\mathbf{Y}, \mathbf{V}, \boldsymbol{\zeta}), \end{aligned} \quad (2.1)$$

where the domains and the ranges of the mappings \mathbf{f} , \mathbf{g} , \mathbf{h} , and \mathbf{k} are as follows:

$$\begin{aligned} \mathbf{f} : \mathbb{R}^r \times \mathbb{R}^{s_0} \times \mathbb{R}^m &\rightarrow \mathbb{R}^r, & \mathbf{h} : \mathbb{R}^r \times \mathbb{R}^{s_0} \times \mathbb{R}^m &\rightarrow \mathbb{R}^{r_0}; \\ \mathbf{g} : \mathbb{R}^{r_0} \times \mathbb{R}^s \times \mathbb{R}^n &\rightarrow \mathbb{R}^s, & \mathbf{k} : \mathbb{R}^{r_0} \times \mathbb{R}^s \times \mathbb{R}^n &\rightarrow \mathbb{R}^{s_0}. \end{aligned} \quad (2.2)$$

To avoid certain technicalities involved in infinite-dimensional representations, we assume that these equations are discretized representations of a stochastic problem that couples two scales, two physical processes, two domains, or a combination thereof. Further, we assume that the data of the first subproblem, which enter this subproblem as physical properties or loadings or both, depend on a finite set of uncertain real parameters denoted as ξ_1, \dots, ξ_m and that the data of the second subproblem depend on a finite set of uncertain real parameters denoted as ζ_1, \dots, ζ_n . We collect these sources of uncertainty into vectors $\boldsymbol{\xi} = (\xi_1, \dots, \xi_m)$ and $\boldsymbol{\zeta} = (\zeta_1, \dots, \zeta_n)$, which we model as random variables defined on a probability triple (Θ, \mathcal{T}, P) with values in \mathbb{R}^m and \mathbb{R}^n , respectively. We refer to $\boldsymbol{\xi}$ and $\boldsymbol{\zeta}$ as *input random variables*.

In the stochastic coupled problem in (2.1), the *solution random variable* \mathbf{U} of the first subproblem depends on the solution random variable \mathbf{V} of the second subproblem via the *coupling random variable* \mathbf{X} . Likewise, the solution random variable \mathbf{V} depends on the solution random variable \mathbf{U} via the coupling random variable \mathbf{Y} .

Thus, to solve this stochastic coupled problem, it is necessary to find the random variables \mathbf{U} and \mathbf{V} defined on (Θ, \mathcal{T}, P) and with values in \mathbb{R}^r and \mathbb{R}^s such that (2.1) is satisfied under the assumption that the stochastic coupled problem is well posed.

For example, if a fluid-structure interaction problem was considered, the stochastic coupled problem in (2.1) could collect the fluid and the structural subproblem; \mathbf{U} and \mathbf{V} could be the solution fields required to describe the states of the fluid and the structure; and \mathbf{X} and \mathbf{Y} could be the traces of the pressure field of the fluid and the velocity field of the structure on the shared fluid-structure interface.

2.2. Partitioned solution. We assume that iterative methods and associated solvers already exist for the solution of each subproblem; therefore, to solve the stochastic coupled problem, we consider a *partitioned method* that reuses these iterative methods as steps in a global iterative method built around them. Here, we assume that each of these iterative methods is based on the reformulation of the associated subproblem as a fixed-point problem as follows:

$$\begin{aligned} \mathbf{U} &= \mathbf{a}(\mathbf{U}, \mathbf{X}, \boldsymbol{\xi}), & \mathbf{Y} &= \mathbf{h}(\mathbf{U}, \mathbf{X}, \boldsymbol{\xi}); \\ \mathbf{V} &= \mathbf{b}(\mathbf{Y}, \mathbf{V}, \boldsymbol{\zeta}), & \mathbf{X} &= \mathbf{k}(\mathbf{Y}, \mathbf{V}, \boldsymbol{\zeta}), \end{aligned} \quad (2.3)$$

where the domains and the ranges of the mappings \mathbf{a} and \mathbf{b} are as follows:

$$\begin{aligned} \mathbf{a} &: \mathbb{R}^r \times \mathbb{R}^{s_0} \times \mathbb{R}^m \rightarrow \mathbb{R}^r; \\ \mathbf{b} &: \mathbb{R}^{r_0} \times \mathbb{R}^s \times \mathbb{R}^n \rightarrow \mathbb{R}^s. \end{aligned} \quad (2.4)$$

These reformulations can be obtained in several ways, for example, by setting

$$\begin{cases} \mathbf{a}(\mathbf{U}, \mathbf{X}, \boldsymbol{\xi}) = \mathbf{U} - \mathbf{f}(\mathbf{U}, \mathbf{X}, \boldsymbol{\xi}) \\ \mathbf{b}(\mathbf{Y}, \mathbf{V}, \boldsymbol{\zeta}) = \mathbf{V} - \mathbf{g}(\mathbf{Y}, \mathbf{V}, \boldsymbol{\zeta}) \end{cases} \quad (\text{simplest}),$$

$$\begin{cases} \mathbf{a}(\mathbf{U}, \mathbf{X}, \boldsymbol{\xi}) = \mathbf{U} - \omega \mathbf{f}(\mathbf{U}, \mathbf{X}, \boldsymbol{\xi}) \\ \mathbf{b}(\mathbf{Y}, \mathbf{V}, \boldsymbol{\zeta}) = \mathbf{V} - \varsigma \mathbf{g}(\mathbf{Y}, \mathbf{V}, \boldsymbol{\zeta}) \end{cases} \quad (\text{linear relaxation}),$$

$$\begin{cases} \mathbf{a}(\mathbf{U}, \mathbf{X}, \boldsymbol{\xi}) = \mathbf{U} - [\mathbf{D}_u \mathbf{f}(\mathbf{U}, \mathbf{X}, \boldsymbol{\xi})]^{-1} (\mathbf{f}(\mathbf{U}, \mathbf{X}, \boldsymbol{\xi})) \\ \mathbf{b}(\mathbf{Y}, \mathbf{V}, \boldsymbol{\zeta}) = \mathbf{V} - [\mathbf{D}_v \mathbf{g}(\mathbf{Y}, \mathbf{V}, \boldsymbol{\zeta})]^{-1} (\mathbf{g}(\mathbf{Y}, \mathbf{V}, \boldsymbol{\zeta})) \end{cases} \quad (\text{Newton's method}),$$

among other ways, including nonlinear relaxation and operator splitting. We then consider the solution of the stochastic coupled problem by a *Gauss-Seidel* partitioned

method, using suitable initial values \mathbf{U}^0 , \mathbf{V}^0 , and \mathbf{X}^0 , as follows:

$$\begin{aligned} \mathbf{U}^\ell &= \mathbf{a}(\mathbf{U}^{\ell-1}, \mathbf{X}^{\ell-1}, \boldsymbol{\xi}), & \mathbf{Y}^\ell &= \mathbf{h}(\mathbf{U}^\ell, \mathbf{X}^{\ell-1}, \boldsymbol{\xi}); \\ \mathbf{V}^\ell &= \mathbf{b}(\mathbf{Y}^\ell, \mathbf{V}^{\ell-1}, \boldsymbol{\zeta}), & \mathbf{X}^\ell &= \mathbf{k}(\mathbf{Y}^\ell, \mathbf{V}^\ell, \boldsymbol{\zeta}). \end{aligned} \quad (2.5)$$

This is not the only partitioned method available; however, for simplicity, we employ only this method in this work. We note that although we adopt this Gauss-Seidel partitioned method, the proposed hybrid method can be used with other partitioned methods, such as Jacobi, relaxation, and Newton iterative methods.

Next, we first describe elementary implementations of the partitioned method in (2.5) using either solely the Monte Carlo sampling method or solely spectral methods, and we then introduce the proposed hybrid method.

2.3. Monte Carlo sampling method. A typical implementation of (2.5) using solely the Monte Carlo sampling method begins by generating an ensemble of independent and identically distributed (i.i.d.) samples $\{(\boldsymbol{\xi}(\theta_k), \boldsymbol{\zeta}(\theta_k)), 1 \leq k \leq \nu\}$ of the input random variables. Then, a sequence of representations of the solution and coupling random variables is computed in the form of a sequence of corresponding ensembles of i.i.d. samples $\{(\mathbf{U}^\ell(\theta_k), \mathbf{V}^\ell(\theta_k), \mathbf{X}^\ell(\theta_k), \mathbf{Y}^\ell(\theta_k)), 1 \leq k \leq \nu\}$. Specifically, the subproblems are solved in the sequence determined by (2.5) in a manner wherein each subproblem is solved at each iteration using the Monte Carlo sampling method to update the samples of the solution and coupling random variables determined by this subproblem. Thus, at iteration ℓ , the first subproblem is solved,

$$\begin{aligned} \mathbf{U}^\ell(\theta_k) &= \mathbf{a}(\mathbf{U}^{\ell-1}(\theta_k), \mathbf{X}^{\ell-1}(\theta_k), \boldsymbol{\xi}(\theta_k)), \\ \mathbf{Y}^\ell(\theta_k) &= \mathbf{h}(\mathbf{U}^\ell(\theta_k), \mathbf{X}^{\ell-1}(\theta_k), \boldsymbol{\xi}(\theta_k)), \end{aligned} \quad 1 \leq k \leq \nu, \quad (2.6)$$

to obtain the representation of the solution and coupling random variables determined by this subproblem as the ensemble of i.i.d. samples

$$\{(\mathbf{U}^\ell(\theta_k), \mathbf{Y}^\ell(\theta_k)), 1 \leq k \leq \nu\}; \quad (2.7)$$

next, the second subproblem is solved,

$$\begin{aligned} \mathbf{V}^\ell(\theta_k) &= \mathbf{b}(\mathbf{Y}^\ell(\theta_k), \mathbf{V}^{\ell-1}(\theta_k), \boldsymbol{\xi}(\theta_k)), \\ \mathbf{X}^\ell(\theta_k) &= \mathbf{k}(\mathbf{Y}^\ell(\theta_k), \mathbf{V}^\ell(\theta_k), \boldsymbol{\zeta}(\theta_k)), \end{aligned} \quad 1 \leq k \leq \nu, \quad (2.8)$$

to obtain the representation of the solution and coupling random variables determined by this subproblem by the ensemble of i.i.d. samples

$$\{(\mathbf{V}^\ell(\theta_k), \mathbf{X}^\ell(\theta_k)), 1 \leq k \leq \nu\}. \quad (2.9)$$

Once the ensembles in (2.7) and (2.9) have converged with respect to the number of iterations, statistical descriptors of the solution and coupling random variables can be deduced therefrom using statistical estimation methods.

We note that this implementation is equivalent to solving the coupled problem for each sample $(\boldsymbol{\xi}(\theta_k), \boldsymbol{\zeta}(\theta_k))$ of the input random variables; such an equivalent implementation can be expected to require less storage, and it also offers the possibility of adjusting the number of iterations for each sample as required to reach convergence.

2.4. Spectral method. A typical implementation of (2.5) using solely spectral methods involves the computation of a sequence of representations of the solution and coupling random variables in the form of a sequence of polynomial chaos expansions $\mathbf{U}^{\ell,p}$, $\mathbf{V}^{\ell,p}$, $\mathbf{X}^{\ell,p}$, and $\mathbf{Y}^{\ell,p}$. Specifically, the subproblems are solved in the sequence determined by (2.5) in a manner wherein each subproblem is solved at each iteration using a spectral method to update the polynomial chaos expansions of those solution and coupling random variables that are determined by this subproblem. Thus, at iteration ℓ , the first subproblem is solved, written as follows:

$$\mathbf{U}^{\ell,p} = \mathbf{a}^p(\mathbf{U}^{\ell-1,p}, \mathbf{X}^{\ell-1,p}, \boldsymbol{\xi}), \quad \mathbf{Y}^{\ell,p} = \mathbf{h}^p(\mathbf{U}^{\ell,p}, \mathbf{X}^{\ell-1,p}, \boldsymbol{\xi}), \quad (2.10)$$

to obtain the representation of the solution and coupling random variables determined by this subproblem by polynomial chaos expansions

$$\mathbf{U}^{\ell,p} = \sum_{|\boldsymbol{\alpha}|=0}^p \psi_{\boldsymbol{\alpha}}(\boldsymbol{\xi}, \boldsymbol{\zeta}) \mathbf{u}^{\ell,\boldsymbol{\alpha}}, \quad \mathbf{Y}^{\ell,p} = \sum_{|\boldsymbol{\alpha}|=0}^p \psi_{\boldsymbol{\alpha}}(\boldsymbol{\xi}, \boldsymbol{\zeta}) \mathbf{y}^{\ell,\boldsymbol{\alpha}}; \quad (2.11)$$

next, the second subproblem is solved using a spectral method, written as follows:

$$\mathbf{V}^{\ell,p} = \mathbf{b}^p(\mathbf{Y}^{\ell,p}, \mathbf{V}^{\ell-1,p}, \boldsymbol{\zeta}), \quad \mathbf{X}^{\ell,p} = \mathbf{k}^p(\mathbf{Y}^{\ell,p}, \mathbf{V}^{\ell,p}, \boldsymbol{\zeta}), \quad (2.12)$$

to obtain the representation of the solution and coupling random variables determined by this subproblem by polynomial chaos expansions

$$\mathbf{V}^{\ell,p} = \sum_{|\boldsymbol{\alpha}|=0}^p \psi_{\boldsymbol{\alpha}}(\boldsymbol{\xi}, \boldsymbol{\zeta}) \mathbf{v}^{\ell,\boldsymbol{\alpha}}, \quad \mathbf{X}^{\ell,p} = \sum_{|\boldsymbol{\alpha}|=0}^p \psi_{\boldsymbol{\alpha}}(\boldsymbol{\xi}, \boldsymbol{\zeta}) \mathbf{x}^{\ell,\boldsymbol{\alpha}}. \quad (2.13)$$

Here, $\{\psi_{\boldsymbol{\alpha}}, \boldsymbol{\alpha} \in \mathbb{N}^{m+n}\}$ is a suitable basis of functions from \mathbb{R}^{m+n} into \mathbb{R} ; in this work, we employ bases that consist of orthonormal polynomials, which is precisely why we refer to the expansions in (2.11) and (2.13) as *polynomial chaos expansions*. Once the polynomial chaos expansions in (2.11) and (2.13) have converged with respect to the number of iterations, statistical descriptors of the solution and coupling random variables can be deduced therefrom using statistical estimation methods.

We note that although our notations do not express a dependence of p on the subproblem or on ℓ , the subset of polynomial chaos used to construct the finite-dimensional representations can be allowed to depend on the subproblem and on ℓ .

2.5. Hybrid method. We propose the following hybrid method. As in the Monte Carlo sampling method described previously, first, we generate an ensemble of i.i.d. samples $\{(\boldsymbol{\xi}(\theta_k), \boldsymbol{\zeta}(\theta_k)), 1 \leq k \leq \nu\}$ of the input random variables. Then, as in the Monte sampling method described previously, we compute a sequence of representations of the solution and coupling random variables in the form of a sequence of corresponding ensembles of samples $\{(\widehat{\mathbf{U}}^{\ell}(\theta_k), \widehat{\mathbf{V}}^{\ell}(\theta_k), \widehat{\mathbf{X}}^{\ell}(\theta_k), \widehat{\mathbf{Y}}^{\ell}(\theta_k)), 1 \leq k \leq \nu\}$. However, in contrast to the Monte Carlo sampling method described previously, we now allow each subproblem at each iteration to be solved using the most computationally efficient Monte Carlo sampling or spectral method to update these samples.

Because truncations of expansions involved in implementations of spectral methods most often result in approximation errors, the sequence of ensembles of samples determined by the proposed hybrid method will most often be only an approximation of the sequence determined by the Monte Carlo sampling method described previously; therefore, we use a hat superscript to distinguish between these sequences.

In the following, we outline an implementation of the proposed hybrid method wherein we solve the first subproblem at each iteration using the Monte Carlo sampling method and the second subproblem at each iteration using a spectral method; nevertheless, we note that variants of this implementation can be easily conceived, such as variants that interchange the role of the subproblems. Thus, at iteration ℓ , we solve the first subproblem using the Monte Carlo sampling method,

$$\begin{aligned}\widehat{\mathbf{U}}^\ell(\theta_k) &= \mathbf{a}(\widehat{\mathbf{U}}^{\ell-1}(\theta_k), \widehat{\mathbf{X}}^{\ell-1}(\theta_k), \boldsymbol{\xi}(\theta_k)), \\ \widehat{\mathbf{Y}}^\ell(\theta_k) &= \mathbf{h}(\widehat{\mathbf{U}}^\ell(\theta_k), \widehat{\mathbf{X}}^{\ell-1}(\theta_k), \boldsymbol{\xi}(\theta_k)),\end{aligned}\quad 1 \leq k \leq \nu, \quad (2.14)$$

to obtain the representation of the solution and coupling random variables determined by this subproblem by the ensemble of samples

$$\{(\widehat{\mathbf{U}}^\ell(\theta_k), \widehat{\mathbf{Y}}^\ell(\theta_k)), 1 \leq k \leq \nu\}. \quad (2.15)$$

Next, we solve the second subproblem using a spectral method. For this purpose, we first use a dimension-reduction technique to characterize the random variables on which the second subproblem depends by a *reduced-dimensional representation*: we approximate the ensemble of samples $\{\mathbf{Q}^\ell(\theta_k) = (\widehat{\mathbf{Y}}^\ell(\theta_k), \widehat{\mathbf{V}}^{\ell-1}(\theta_k)), 1 \leq k \leq \nu\}$ by the ensemble of samples $\{\mathbf{Q}^{\ell,d}(\theta_k) = (\widehat{\mathbf{Y}}^{\ell,d}(\theta_k), \widehat{\mathbf{V}}^{\ell-1,d}(\theta_k)), 1 \leq k \leq \nu\}$ obtained through the truncation of a Karhunen-Loève (KL) decomposition after d terms [1, 2]:

$$\mathbf{Q}^{\ell,d}(\theta_k) = \bar{\mathbf{q}}^\ell + \sum_{j=1}^d \sqrt{\lambda_j^\ell} \eta_j^\ell(\theta_k) \boldsymbol{\varphi}^{\ell,j}, \quad 1 \leq k \leq \nu. \quad (2.16)$$

Because of this characterization of the random variables on which the second subproblem depends by a reduced-dimensional representation, we do not need to construct the required ensemble of samples $\{(\widehat{\mathbf{V}}^\ell(\theta_k), \widehat{\mathbf{X}}^\ell(\theta_k)), 1 \leq k \leq \nu\}$ as a transformation of the ensemble of samples $\{(\boldsymbol{\xi}(\theta_k), \boldsymbol{\zeta}(\theta_k)), 1 \leq k \leq \nu\}$ as in (2.12) and (2.13), but we can construct this ensemble of samples as a transformation of the ensemble of samples $\{(\boldsymbol{\eta}^\ell(\theta_k), \boldsymbol{\zeta}(\theta_k)), 1 \leq k \leq \nu\}$, wherein $\boldsymbol{\eta}^\ell(\theta_k) = (\eta_1^\ell(\theta_k), \dots, \eta_d^\ell(\theta_k))$ and $\boldsymbol{\zeta}(\theta_k) = (\zeta_1(\theta_k), \dots, \zeta_n(\theta_k))$; thus, we can solve the second subproblem using a spectral method in a reduced-dimensional space of dimension $d + n$, written as

$$\widehat{\mathbf{V}}^{\ell,d,q} = \widehat{\mathbf{b}}^{\ell,d,q}(\widehat{\mathbf{Y}}^{\ell,d}, \widehat{\mathbf{V}}^{\ell-1,d}, \boldsymbol{\zeta}), \quad \widehat{\mathbf{X}}^{\ell,d,q} = \widehat{\mathbf{h}}^{\ell,d,q}(\widehat{\mathbf{Y}}^{\ell,d}, \widehat{\mathbf{V}}^{\ell,d,q}, \boldsymbol{\zeta}), \quad (2.17)$$

to obtain a representation of the solution and coupling random variables determined by this subproblem by polynomial chaos expansions

$$\widehat{\mathbf{V}}^{\ell,d,q} = \sum_{|\boldsymbol{\beta}|=0}^q \Gamma_{\boldsymbol{\beta}}^\ell(\boldsymbol{\eta}^\ell, \boldsymbol{\zeta}) \widehat{\mathbf{v}}^{\ell,\boldsymbol{\beta}}, \quad \widehat{\mathbf{X}}^{\ell,d,q} = \sum_{|\boldsymbol{\beta}|=0}^q \Gamma_{\boldsymbol{\beta}}^\ell(\boldsymbol{\eta}^\ell, \boldsymbol{\zeta}) \widehat{\mathbf{x}}^{\ell,\boldsymbol{\beta}}, \quad (2.18)$$

where $\{\Gamma_{\boldsymbol{\beta}}^\ell, \boldsymbol{\beta} \in \mathbb{N}^{d+n}\}$ is a suitable basis of functions from \mathbb{R}^{d+n} into \mathbb{R} . The global approximation by polynomial chaos expansions in (2.18) provides the approximation in terms of samples as $\widehat{\mathbf{V}}^\ell(\theta_k) \equiv \widehat{\mathbf{V}}^{\ell,d,q}(\theta_k)$ and $\widehat{\mathbf{X}}^\ell(\theta_k) \equiv \widehat{\mathbf{X}}^{\ell,d,q}(\theta_k)$, that is,

$$\widehat{\mathbf{V}}^\ell(\theta_k) = \sum_{|\boldsymbol{\beta}|=0}^q \Gamma_{\boldsymbol{\beta}}^\ell(\boldsymbol{\eta}^\ell(\theta_k), \boldsymbol{\zeta}(\theta_k)) \widehat{\mathbf{v}}^{\ell,\boldsymbol{\beta}}, \quad \widehat{\mathbf{X}}^\ell(\theta_k) = \sum_{|\boldsymbol{\beta}|=0}^q \Gamma_{\boldsymbol{\beta}}^\ell(\boldsymbol{\eta}^\ell(\theta_k), \boldsymbol{\zeta}(\theta_k)) \widehat{\mathbf{x}}^{\ell,\boldsymbol{\beta}}, \quad (2.19)$$

to obtain the required representation of the solution and coupling random variables determined by this subproblem by the ensemble of samples

$$\{(\widehat{\mathbf{V}}^\ell(\theta_k), \widehat{\mathbf{X}}^\ell(\theta_k)), 1 \leq k \leq \nu\}. \quad (2.20)$$

Although our notations do not express a potential dependence of d and q on ℓ , we note that these parameters may depend on the iteration.

2.6. Discretization error incurred by hybrid method. When statistical descriptors of the solution are computed, the proposed hybrid method incurs discretization errors that are primarily controlled by the following *discretization parameters*: the number of samples ν , the number of iterations, and the *dimension* d and *order* q . The number of samples ν determines the *sampling error* that is incurred when mathematical statistics methods are used to estimate statistical descriptors of the solution random variables from the only finite number of samples provided by the proposed hybrid method. The number of iterations determines the *iteration error* that remains after halting the iterative method after only a finite number of iterations. The dimension d and order q determine the *truncation error* that is introduced owing to the solution at each iteration of the second subproblem using a spectral method in only a reduced-dimensional space for only a truncated polynomial chaos expansion. For example, when the expectation value $\mu_U = \int_{\Theta} U dP$ of the solution random variable U is approximated by the estimate $\frac{1}{\nu} \sum_{k=1}^{\nu} \widehat{U}^\ell(\theta_k)$, the discretization error, that is, $\mu_U - \frac{1}{\nu} \sum_{k=1}^{\nu} \widehat{U}^\ell(\theta_k)$, can be decomposed as follows:

$$\underbrace{\mu_U - \frac{1}{\nu} \sum_{k=1}^{\nu} U(\theta_k)}_{\text{sampling error}} + \underbrace{\frac{1}{\nu} \sum_{k=1}^{\nu} (U(\theta_k) - U^\ell(\theta_k))}_{\text{iteration error}} + \underbrace{\frac{1}{\nu} \sum_{k=1}^{\nu} (U^\ell(\theta_k) - \widehat{U}^\ell(\theta_k))}_{\text{truncation error}}. \quad (2.21)$$

2.7. Effectiveness of hybrid method. The main feature of the proposed hybrid method is that it allows uncertainties to be accurately propagated through coupled problems and yet can be implemented as a wrapper around separate methods for the propagation of uncertainties through subproblems, where the most computationally efficient Monte Carlo sampling or spectral method can be used.

The implementation of the proposed hybrid method given by (2.14)–(2.20) can be expected to facilitate a computationally efficient solution of the stochastic coupled problem in (2.1) especially when the first subproblem has a “very high dimension,” that is, $m+n$ is large, but the second subproblem has a “low or moderate dimension,” that is, $d+n$ is small or moderate. Indeed, the proposed hybrid method can then be expected to be able to combine the computational efficiency of the Monte Carlo sampling method for solving problems of “very high dimension” with the computational efficiency of spectral methods for solving problems of “low or moderate dimension.”

For the first subproblem to be of “very high dimension,” it suffices that its data depend on a very large number m of sources of uncertainty. For the second subproblem to be of “low or moderate dimension,” it is necessary that its data depend on only a small or moderate number n of sources of uncertainty and that the truncated KL decomposition is able to accurately characterize the random variables on which the second subproblem depends by a representation of only low or moderate dimension d .

3. Implementation: computational construction of polynomial chaos.

Here, we detail how the proposed hybrid method enables the solution of subproblems

using spectral methods: we detail how the solution of the second subproblem of the model problem in (2.1) can be implemented using spectral methods as in (2.16)–(2.20).

The main challenge is that whereas the context for the solution of a stochastic problem by a spectral method is usually set by a characterization of the sources of uncertainty in terms of their probability distribution, the context is set here by a characterization of the sources of uncertainty in terms of an ensemble of samples.

Depending on the specific spectral method that is chosen, the implementation of this spectral method typically requires that various algorithmic constituents be defined, such as second-order descriptors, polynomial chaos, and projection and other methods. When the sources of uncertainty are characterized by their probability distribution, the definitions of these algorithmic constituents usually involve expectation values that are themselves defined in terms of integrals with respect to this probability distribution; alternatively, after a suitable transformation of the sources of uncertainty, integrals with respect to Gaussian or other “labeled” probability distributions are often relied upon; for details, please refer to [7, 11, 19].

However, here, the sources of uncertainty are characterized by an ensemble of samples; hence, the algorithmic constituents cannot be immediately defined in the manner mentioned previously, but two alternative approaches can be adopted. First, nonparametric or mathematical statistics methods can be applied to fit a probability distribution to this ensemble of samples, for example, by adopting the approaches in [14–16], after which the usual definitions of the algorithmic constituents can be relied upon again. Alternatively, the expectation values involved in the definitions of the algorithmic constituents can be replaced with sample averages. The former approach can be expected to entail a much higher computational cost than the latter approach because fitting a probability distribution to an ensemble of samples is computationally very expensive. Further, the choice between these approaches can be expected to affect the accuracy of the approximate solution that will be provided by the resulting spectral method because this choice essentially determines the Hilbert-space projections with reference to which this approximate solution will be constructed.

In this work, we adopt the approach involving the use of sample averages. Below, we show how this use of sample averages facilitates in turn the use of computational linear algebra methods for obtaining the requisite polynomial chaos.

3.1. Objective. We describe a computational construction of a basis $\{\Gamma_{\beta}, 0 \leq |\beta| \leq q\}$ of z -variate polynomials Γ_{β} that are of increasing order and orthonormal in an inner product defined as a sample average with reference to an ensemble $\{\chi(\theta_k), 1 \leq k \leq \nu\}$ of samples $\chi(\theta_k)$ in \mathbb{R}^z , that is, these polynomial chaos are such that

$$\frac{1}{\nu} \sum_{k=1}^{\nu} \Gamma_{\beta}(\chi(\theta_k)) \Gamma_{\gamma}(\chi(\theta_k)) = \delta_{\beta\gamma}, \quad 0 \leq |\beta|, |\gamma| \leq q. \quad (3.1)$$

3.2. Interpretation. In the frame of the proposed hybrid method, we consider $\{\chi(\theta_k), 1 \leq k \leq \nu\}$ as an ensemble of samples of the sources of uncertainty that enter a subproblem solved by a spectral method at some iteration. For example, with reference to (2.18), at iteration ℓ , each sample $\chi(\theta_k) = (\boldsymbol{\eta}^{\ell}(\theta_k), \zeta(\theta_k))$ could collect the components of the samples $\boldsymbol{\eta}^{\ell}(\theta_k)$ and $\zeta(\theta_k)$ with $z = d + n$; then, the polynomial chaos Γ_{β} would be needed to build the polynomial chaos expansions $\widehat{\mathbf{V}}^{\ell, d, q}$ and $\widehat{\mathbf{X}}^{\ell, d, q}$.

3.3. Computational construction. We refer to elements $\beta = (\beta_1, \dots, \beta_z)$ of \mathbb{N}^z as *multi-indices*. A (multivariate) *monomial* χ^{β} associated with a multi-index β is then a function from \mathbb{R}^z into \mathbb{R} defined by $\chi^{\beta} = \chi_1^{\beta_1} \times \dots \times \chi_z^{\beta_z}$. We refer to $|\beta| =$

$\beta_1 + \dots + \beta_z$ as the *order* of $\boldsymbol{\chi}^\beta$. A (multivariate) *polynomial* is a function from \mathbb{R}^z into \mathbb{R} that maps any $\boldsymbol{\chi}$ to a finite sum $\sum_{\beta} c_{\beta} \boldsymbol{\chi}^{\beta}$ with real coefficients c_{β} . Let $\mathcal{P}_z^q = \{\pi : \boldsymbol{\chi} = (\chi_1, \dots, \chi_z) \mapsto \pi(\boldsymbol{\chi}) = \sum_{|\beta|=0}^q c_{\beta} \boldsymbol{\chi}^{\beta}\}$ be the space of all polynomials in z variables with order at most q . We denote by $\mu = (z + q)!/z!q!$ the dimension of \mathcal{P}_z^q .

There are several ways of constructing for the space \mathcal{P}_z^q a basis of z -variate polynomials Γ_{β} that are of increasing order and orthonormal in that (3.1) is fulfilled. We describe a computational construction that involves a QR factorization; we refer to [8, 12, 17] for alternative methods involving singular value decompositions and Cholesky factorizations. First, we compute the $\nu \times \mu$ -dimensional matrix $[M]$ whose entries $M_{k\beta}$ are the values taken by the monomials $\boldsymbol{\chi}^{\beta}$ at the samples $\boldsymbol{\chi}(\theta_k)$:

$$M_{k\beta} = (\boldsymbol{\chi}(\theta_k))^{\beta} = (\chi_1(\theta_k))^{\beta_1} \times \dots \times (\chi_z(\theta_k))^{\beta_z}, \quad (3.2)$$

where we sort the monomials $\boldsymbol{\chi}^{\beta}$ that determine the columns of $[M]$ in graded lexicographical order. Next, we compute the thin QR factorization

$$[M] = [QR], \quad (3.3)$$

where $[Q]$ is a $\nu \times \mu$ -dimensional orthogonal matrix and $[R]$ a μ -dimensional square upper triangular matrix [9]. If $[M]$ has full column rank and the diagonal entries of $[R]$ are required to be positive, this factorization exists and is unique [9]. Subsequently, we invert $[R]$ to obtain the μ -dimensional square upper triangular matrix

$$[A] = \sqrt{\nu}[R]^{-1}, \quad (3.4)$$

which provides the coefficients of the required polynomial chaos Γ_{β} as follows:

$$\Gamma_{\beta}(\boldsymbol{\chi}) = \sum_{\gamma \leq \beta} A_{\gamma\beta} \boldsymbol{\chi}^{\gamma}, \quad 0 \leq |\beta| \leq q. \quad (3.5)$$

Indeed, upon introducing the $\nu \times \mu$ -dimensional matrix $[\Gamma]$ whose entries $\Gamma_{k\beta} = \Gamma_{\beta}(\boldsymbol{\chi}(\theta_k))$ are the values taken by the polynomial chaos Γ_{β} at the samples $\boldsymbol{\chi}(\theta_k)$, that is, $[\Gamma] = [MA]$, we obtain $\frac{1}{\nu} \sum_{k=1}^{\nu} [\Gamma^T \Gamma] = \frac{1}{\nu} \sum_{k=1}^{\nu} [A^T M^T M A] = [Q^T Q] = [I]$; hence, the required orthonormality property (3.1) is fulfilled (here, $[I]$ is the z -dimensional identity matrix). Finally, substituting (3.3) and (3.4) in $[\Gamma] = [MA]$ shows that the QR factorization provides $[\Gamma] = \sqrt{\nu}[Q]$, that is, the entries $Q_{k\beta}$ of $[Q]$ provide the values $\Gamma_{\beta}(\boldsymbol{\chi}(\theta_k)) = \sqrt{\nu}Q_{k\beta}$ taken by the polynomial chaos Γ_{β} at the samples $\boldsymbol{\chi}(\theta_k)$.

We note that the computational cost and the storage requirements associated with the QR factorization in (3.3) can be expected to increase rapidly with the dimension z .

4. Realization for a stochastic multiphysics problem.

4.1. Problem formulation. We consider the two-dimensional plane-strain elastic bending of a microbridge, that is, a clamped-clamped micrometer-scale beam, under electrostatic actuation (Fig. 4.1). Let the microbridge be coated with a thin conductive layer and be surrounded by a rectangular electrode. Then, the application of a potential difference between the microbridge and electrode causes charges to distribute themselves on the surfaces of the microbridge and electrode. The electrostatic field introduced owing to this surface distribution of charges results in an electrostatic force on the surfaces of the microbridge and electrode, thus forcing the microbridge to bend. The bending of the microbridge in turn causes the charges to redistribute themselves and, consequently, their resultant electrostatic force and the

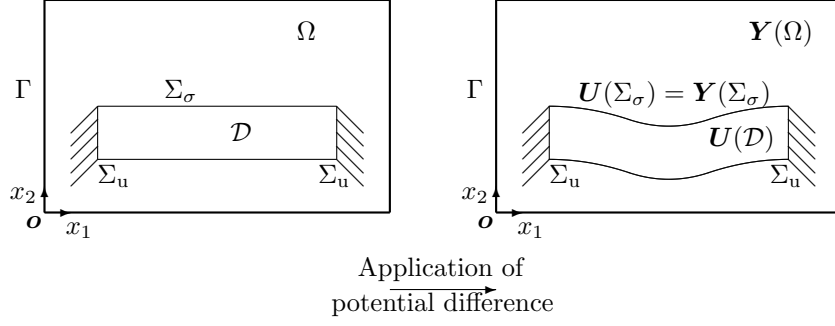


FIG. 4.1. Schematic representation of the problem.

bending of the microbridge to change, thus indicating that the problem is a coupled elasticity/electrostatics problem. Below, we incorporate uncertainties in the elastic and electrostatic material properties of this coupled elasticity/electrostatics problem, and we demonstrate the proposed hybrid method through its application to the determination of the random displacement of the microbridge induced by the application of a potential difference between the microbridge and the electrode.

4.2. Random elasticity tensor and electrical permittivity. We model the elasticity tensor field in \mathcal{D} by the random field $\{[a(\mathbf{x}, \boldsymbol{\xi})], \mathbf{x} \in \mathcal{D}\}$. We assume this random field to be isotropic and determined by the random Young modulus field $\{E(\mathbf{x}, \boldsymbol{\xi}), \mathbf{x} \in \mathcal{D}\}$ and random Poisson coefficient field $\{\nu(\mathbf{x}, \boldsymbol{\xi}), \mathbf{x} \in \mathcal{D}\}$ such that

$$E(\mathbf{x}, \boldsymbol{\xi}) = \bar{E} \left(1 + \delta_E \sum_{j=1}^{m_E} \sqrt{\lambda_{E,j}} \sqrt{3} \xi_j \varphi_E^j(\mathbf{x}) \right), \quad (4.1)$$

$$\nu(\mathbf{x}, \boldsymbol{\xi}) = \bar{\nu} \left(1 + \delta_\nu \sum_{j=1}^{m_\nu} \sqrt{\lambda_{\nu,j}} \sqrt{3} \xi_{m_E+j} \varphi_\nu^j(\mathbf{x}) \right). \quad (4.2)$$

We model the electrical permittivity in Ω by the random variable $\epsilon_0(\zeta)$ such that

$$\epsilon_0(\zeta) = \bar{\epsilon}_0 (1 + \delta_{\epsilon_0} \sqrt{3} \zeta). \quad (4.3)$$

Here, the random variables ξ_j and ζ are statistically independent uniform random variables defined on (Θ, \mathcal{T}, P) with values in $[-1, 1]$. Hence, the random variable ϵ_0 has mean value $\bar{\epsilon}_0$ and coefficient of variation δ_{ϵ_0} . Further, $\lambda_{E,j}$ and φ_E^j ($\lambda_{\nu,j}$ and φ_ν^j) are the eigenvalues and eigenmodes of the eigenproblem $\mathcal{C}_E(\varphi_E^j) = \lambda_{E,j} \varphi_E^j$ ($\mathcal{C}_\nu(\varphi_\nu^j) = \lambda_{\nu,j} \varphi_\nu^j$), where \mathcal{C}_E and \mathcal{C}_ν are covariance operators with the following kernels:

$$C_E(\mathbf{x}, \tilde{\mathbf{x}}) = \frac{4a_E^2}{\pi^2(x_1 - \tilde{x}_1)^2} \sin^2\left(\frac{\pi(x_1 - \tilde{x}_1)}{2a_E}\right) \frac{4a_E^2}{\pi^2(x_2 - \tilde{x}_2)^2} \sin^2\left(\frac{\pi(x_2 - \tilde{x}_2)}{2a_E}\right), \quad (4.4)$$

$$C_\nu(\mathbf{x}, \tilde{\mathbf{x}}) = \frac{4a_\nu^2}{\pi^2(x_1 - \tilde{x}_1)^2} \sin^2\left(\frac{\pi(x_1 - \tilde{x}_1)}{2a_\nu}\right) \frac{4a_\nu^2}{\pi^2(x_2 - \tilde{x}_2)^2} \sin^2\left(\frac{\pi(x_2 - \tilde{x}_2)}{2a_\nu}\right). \quad (4.5)$$

Here, the parameters a_E and a_ν are the spatial correlation lengths of the random Young modulus and Poisson coefficient fields, respectively. Hence, the random fields thus obtained are such that the random variables $E(\mathbf{x}, \boldsymbol{\xi})$ and $\nu(\mathbf{x}, \boldsymbol{\xi})$ have mean values \bar{E} and $\bar{\nu}$ and coefficients of variation δ_E and δ_ν , respectively, at every position \mathbf{x} ,

at least when the approximation errors introduced owing to the truncation of the expansions after m_E and m_ν terms, respectively, are not taken into account.

We note that δ_E , δ_ν , and δ_{ε_0} must be sufficiently small to ensure positiveness of the Young modulus, boundedness of the Poisson coefficient between -1 and $1/2$, and positiveness of the electrical permittivity, respectively. Further, we acknowledge that our choice of stochastic model is rather arbitrary; in engineering applications, adequate stochastic models can be inferred from experimental data using mathematical statistics methods or constructed using information-theoretic methods [10].

4.3. Stochastic coupled problem. We adopt a large displacements/large deformations formulation, which accounts for the transport of tractions, volume elements, and surface elements between the original and deformed configurations using the standard relations involving the deformation tensor, jacobian determinant, and dilation tensor of the displacement; for details, refer to [3]. To enable this transport, we extend the displacement \mathbf{U} in the domain \mathcal{D} occupied by the microbridge to obtain a corresponding displacement \mathbf{Y} in the exterior domain \mathcal{D} ; we use as the extension operator the standard harmonic extension operator, which involves solving Laplace's equation under Dirichlet boundary conditions. Thus, we consider the stochastic coupled problem that involves finding the random displacement \mathbf{U} , the random displacement \mathbf{Y} , and the random potential Φ defined on (Θ, \mathcal{T}, P) such that

$$\left\{ \begin{array}{ll} -\operatorname{div}_{\mathbf{x}}[F(\mathbf{U})S(\mathbf{U})] = \mathbf{0} & \text{in } \mathcal{D}, \\ [E(\mathbf{U})] = \frac{1}{2}[F(\mathbf{U})^T F(\mathbf{U}) - I] & \text{in } \mathcal{D}, \\ [S(\mathbf{U})] = \llbracket a(\cdot, \boldsymbol{\xi}) \rrbracket([E(\mathbf{U})]) & \text{in } \mathcal{D}, \\ \mathbf{U} = \mathbf{0} & \text{on } \Sigma_{\mathbf{u}}, \\ [F(\mathbf{U})S(\mathbf{U})]\mathbf{n} = \frac{\varepsilon_0(\zeta)}{2} \left(\frac{(\nabla_{\mathbf{x}}\Phi^T[C(\mathbf{Y})]^{-1}\mathbf{n})}{\|[F(\mathbf{Y})]^{-T}(\mathbf{n})\|} \right)^2 j(\mathbf{U})[F(\mathbf{U})]^{-T}\mathbf{n} & \text{on } \Sigma_{\sigma}; \\ -\operatorname{div}_{\mathbf{x}}[D_{\mathbf{x}}\mathbf{Y}] = \mathbf{0} & \text{in } \Omega, \\ \mathbf{Y} = \mathbf{0} & \text{on } \Gamma, \\ \mathbf{Y} = \mathbf{u} & \text{on } \Sigma; \\ -\operatorname{div}_{\mathbf{x}}(j(\mathbf{Y})[C(\mathbf{Y})]^{-1}\nabla_{\mathbf{x}}\Phi) = 0 & \text{in } \Omega, \\ \Phi = 0 & \text{on } \Gamma, \\ \Phi = \phi^{\text{ext}} & \text{on } \Sigma. \end{array} \right. \quad (4.6)$$

Here, $[S(\mathbf{U})]$ is the Piola-Kirchhoff tensor; $[E(\mathbf{U})]$ is the Green-Lagrange tensor; and $[F(\mathbf{U})] = [I + D_{\mathbf{x}}\mathbf{U}]$ and $[F(\mathbf{Y})] = [I + D_{\mathbf{x}}\mathbf{Y}]$ are the deformation tensors with corresponding jacobian determinants $j(\mathbf{U}) = \det[F(\mathbf{U})]$ and $j(\mathbf{Y}) = \det[F(\mathbf{Y})]$ and dilatation tensors $[C(\mathbf{U})] = [F(\mathbf{U})^T F(\mathbf{U})]$ and $[C(\mathbf{Y})] = [F(\mathbf{Y})^T F(\mathbf{Y})]$.

The elasticity subproblem in (4.6) expresses mechanical equilibrium in \mathcal{D} , a Dirichlet boundary condition on the portion $\Sigma_{\mathbf{u}}$ of the interface Σ where the microbridge is clamped, a Neumann boundary condition that models the electrostatic pressure on the complementary portion Σ_{σ} , completed by a hyperelastic constitutive equation. The electrostatics subproblem in (4.7) expresses Gauss's law in Ω and Dirichlet boundary conditions on the external boundary Γ and interface $\Sigma = \Sigma_{\mathbf{u}} \cup \Sigma_{\sigma}$, between which a potential difference of ϕ^{ext} is applied. The vector \mathbf{n} is the unit normal vector on the interface Σ , chosen to point outward from \mathcal{D} into Ω .

4.4. Finite element equations. We now develop the finite element (FE) equations for the stochastic coupled problem. We use a mesh of four-node quadrilateral elements in \mathcal{D} and a mesh of three-node triangular elements in Ω .

Throughout the remainder of this paper, we denote by \mathbf{U} the random vector that collects the nodal values of the FE approximation of the displacement in \mathcal{D} and by \mathbf{Y} and Φ the random vectors that collect the nodal values of the FE approximations of the displacement and potential in Ω (please note the reuse of notation: whereas \mathbf{U} and \mathbf{Y} represented the displacement itself in the previous section, they represent the nodal values of the FE approximation of the displacement in this and all following sections). Then, the FE equations—inferred from (4.6) and (4.7) by a standard Galerkin projection—can be written as finding the random vectors \mathbf{U} , $\mathbf{Y} = (\mathbf{Y}_\Omega, \mathbf{Y}_\Sigma)$, and $\Phi = (\Phi_\Omega, \phi_\Sigma)$ defined on (Θ, \mathcal{T}, P) such that

$$\{\mathbf{f}(\mathbf{U}, \mathbf{T}, \xi) = \mathbf{0}, \quad \mathbf{Y}_\Sigma = \mathbf{h}(\mathbf{U}); \quad (4.8)$$

$$\begin{cases} [M_{\Omega\Omega}]\mathbf{Y}_\Omega = -[M_{\Omega\Sigma}]\mathbf{Y}_\Sigma, \\ [K_{\Omega\Omega}(\mathbf{Y})]\Phi_\Omega = -[K_{\Omega\Sigma}(\mathbf{Y})]\phi_\Sigma, \end{cases} \quad \mathbf{T} = \mathbf{k}(\mathbf{Y}, \Phi, \zeta). \quad (4.9)$$

In equation (4.8), which represents the FE approximation of the elasticity subproblem in (4.6), $\mathbf{f}(\mathbf{U}, \mathbf{T}, \xi)$ is the residual obtained by subtracting from the internal nodal forces (corresponding to stresses in the material) the external nodal forces (due to the electrostatic pressure). In equation (4.9), which represents the FE approximation of the electrostatics subproblem in (4.7), $[M]$ and $[K(\mathbf{Y})]$ are the FE approximations of the corresponding differential operators involved in (4.7), and the subscripts Ω and Σ refer to a block partitioning of matrices and vectors that separates nodal values associated with nodes in the interior of Ω from those associated with nodes on Σ .

Because the meshes in \mathcal{D} and Ω need not be compatible on Σ , $\mathbf{Y}_\Sigma = \mathbf{h}(\mathbf{U})$ refers to an orthogonal projection used to transform the nodal values of the displacement in \mathcal{D} into the nodal values of the trace of the corresponding displacement in Ω , and $\mathbf{T} = \mathbf{k}(\mathbf{Y}, \Phi, \zeta)$ is another orthogonal projection used to transform the nodal values of the displacement and potential in Ω into nodal values of the electrostatic pressure on Σ .

4.5. Partitioned solution. We use the Gauss-Seidel partitioned method built around a Newton nonlinear solution method for the elasticity subproblem and linear solution methods for the electrostatics subproblem, written as follows:

$$\{[Z(\mathbf{U}^{\ell-1}, \xi)](\mathbf{U}^\ell - \mathbf{U}^{\ell-1}) = -\mathbf{f}(\mathbf{U}^{\ell-1}, \mathbf{T}^{\ell-1}, \xi), \quad \mathbf{Y}_\Sigma^\ell = \mathbf{h}(\mathbf{U}^\ell); \quad (4.10)$$

$$\begin{cases} [M_{\Omega\Omega}]\mathbf{Y}_\Omega^\ell = -[M_{\Omega\Sigma}]\mathbf{Y}_\Sigma^\ell, \\ [K_{\Omega\Omega}(\mathbf{Y}^\ell)]\Phi_\Omega^\ell = -[K_{\Omega\Sigma}(\mathbf{Y}^\ell)]\phi_\Sigma, \end{cases} \quad \mathbf{T}^\ell = \mathbf{k}(\mathbf{Y}^\ell, \Phi^\ell, \zeta). \quad (4.11)$$

Here, $[Z(\mathbf{U}^{\ell-1}, \xi)]$ is the tangent stiffness matrix, which we infer from the residual vector in (4.8) using the standard approach given in [3].

4.6. Dimension reduction. We describe an implementation of the proposed hybrid method that solves the elasticity subproblem at each iteration using the Monte Carlo sampling method and the electrostatics subproblem at each iteration using a spectral method. Because the electrostatics subproblem depends on the nodal values of the displacement on Σ in the partitioned method in (4.10)–(4.11), we require a reduced-dimensional representation of these nodal values of the displacement on Σ to facilitate the solution of the electrostatics subproblem in a reduced-dimensional space.

Let these nodal values of the displacement on Σ at iteration ℓ be represented by the ensemble of samples

$$\{\widehat{\mathbf{Y}}_{\Sigma}^{\ell}(\theta_k), 1 \leq k \leq \nu\}. \quad (4.12)$$

We construct the reduced-dimensional representation through the truncation of a KL decomposition [1, 2]. First, we compute the sample mean and covariance matrix:

$$\bar{\mathbf{y}}_{\Sigma}^{\ell} = \frac{1}{\nu} \sum_{k=1}^{\nu} \widehat{\mathbf{Y}}_{\Sigma}^{\ell}(\theta_k), \quad [\widehat{\mathbf{C}}_{\mathbf{Y}_{\Sigma}}^{\ell}] = \frac{1}{\nu} \sum_{k=1}^{\nu} \left(\widehat{\mathbf{Y}}_{\Sigma}^{\ell}(\theta_k) - \bar{\mathbf{y}}_{\Sigma}^{\ell} \right) \left(\widehat{\mathbf{Y}}_{\Sigma}^{\ell}(\theta_k) - \bar{\mathbf{y}}_{\Sigma}^{\ell} \right)^{\top}. \quad (4.13)$$

Then, with $[W]$ the Gram matrix of the FE shape functions, we solve the eigenproblem

$$[W^{\top} \widehat{\mathbf{C}}_{\mathbf{Y}_{\Sigma}}^{\ell} W] \boldsymbol{\varphi}_{\Sigma}^{\ell, j} = \lambda_j^{\ell} [W] \boldsymbol{\varphi}_{\Sigma}^{\ell, j} \quad (4.14)$$

to obtain the eigenvalues and eigenmodes required to construct the reduced-dimensional representation as follows:

$$\widehat{\mathbf{Y}}_{\Sigma}^{\ell}(\theta_k) \approx \widehat{\mathbf{Y}}_{\Sigma}^{\ell, d}(\theta_k) = \bar{\mathbf{y}}_{\Sigma}^{\ell} + \sum_{j=1}^d \sqrt{\lambda_j^{\ell}} \eta_j^{\ell}(\theta_k) \boldsymbol{\varphi}_{\Sigma}^{\ell, j}, \quad 1 \leq k \leq \nu, \quad (4.15)$$

where for $j = 1, \dots, d$, the ensembles $\{\eta_j^{\ell}(\theta_k), 1 \leq k \leq \nu\}$ collect the samples $\eta_j^{\ell}(\theta_k)$ in \mathbb{R} such that

$$\eta_j^{\ell}(\theta_k) = \frac{1}{\sqrt{\lambda_j^{\ell}}} \left(\widehat{\mathbf{Y}}_{\Sigma}^{\ell}(\theta_k) - \bar{\mathbf{y}}_{\Sigma}^{\ell} \right)^{\top} [W] \boldsymbol{\varphi}_{\Sigma}^{\ell, j}, \quad 1 \leq k \leq \nu. \quad (4.16)$$

4.7. Computational construction of polynomial chaos. We construct polynomial chaos $\{\Gamma_{\boldsymbol{\beta}}^{\ell}, 0 \leq |\boldsymbol{\beta}| \leq q\}$ using the approach given in Sec. 3. First, we compute the $\nu \times \mu$ -dimensional matrix $[M^{\ell}]$, with $\mu = (d+q)!/d!q!$, such that

$$M_{k\boldsymbol{\beta}}^{\ell} = (\boldsymbol{\eta}^{\ell}(\theta_k))^{\boldsymbol{\beta}} \equiv (\eta_1^{\ell}(\theta_k))^{\beta_1} \times \dots \times (\eta_d^{\ell}(\theta_k))^{\beta_d}, \quad (4.17)$$

where we sort the monomials $(\boldsymbol{\eta}^{\ell})^{\boldsymbol{\beta}}$ that determine the columns of $[M^{\ell}]$ in graded lexicographical order. Then, we compute the thin QR factorization of $[M^{\ell}]$:

$$[M^{\ell}] = [Q^{\ell} R^{\ell}], \quad (4.18)$$

which, after inverting the μ -dimensional square upper triangular matrix $[R^{\ell}]$ to obtain

$$[A^{\ell}] = \sqrt{\nu} [R^{\ell}]^{-1}, \quad (4.19)$$

provides the coefficients of the required polynomial chaos $\Gamma_{\boldsymbol{\beta}}^{\ell}$ as follows:

$$\Gamma_{\boldsymbol{\beta}}^{\ell}(\boldsymbol{\eta}^{\ell}) = \sum_{\boldsymbol{\gamma} \leq \boldsymbol{\beta}} A_{\boldsymbol{\gamma}\boldsymbol{\beta}}^{\ell}(\boldsymbol{\eta}^{\ell}) \boldsymbol{\gamma}, \quad 0 \leq |\boldsymbol{\beta}| \leq q, \quad (4.20)$$

and also provides the $\nu \times \mu$ -dimensional matrix $[\Gamma^{\ell}] = \sqrt{\nu} [Q^{\ell}]$ that collects the values $\Gamma_{k\boldsymbol{\beta}}^{\ell} \equiv \Gamma_{\boldsymbol{\beta}}^{\ell}(\boldsymbol{\eta}^{\ell}(\theta_k))$ taken by the polynomial chaos $\Gamma_{\boldsymbol{\beta}}^{\ell}$ at the samples $\boldsymbol{\eta}^{\ell}(\theta_k)$. Lastly, we compute the $\mu \times \mu \times \mu$ -dimensional moment array $[[c^{\ell}]]$ such that

$$c_{\boldsymbol{\alpha}\boldsymbol{\beta}\boldsymbol{\gamma}}^{\ell} = \frac{1}{\nu} \sum_{k=1}^{\nu} \Gamma_{k\boldsymbol{\alpha}}^{\ell} \Gamma_{k\boldsymbol{\beta}}^{\ell} \Gamma_{k\boldsymbol{\gamma}}^{\ell}, \quad 0 \leq |\boldsymbol{\alpha}|, |\boldsymbol{\beta}|, |\boldsymbol{\gamma}| \leq q. \quad (4.21)$$

4.8. Embedded stochastic projection. We solve the electrostatics subproblem using the standard embedded stochastic projection method [7, 11, 18]. First, we extend the reduced-dimensional representation of the nodal values of the displacement on Σ to obtain a corresponding reduced-dimensional representation of the nodal values of the displacement in Ω :

$$\widehat{\mathbf{Y}}^{\ell,d} = \bar{\mathbf{y}}^\ell + \sum_{j=1}^d \sqrt{\lambda_j^\ell} \eta_j^\ell \boldsymbol{\varphi}^{\ell,j}, \quad \begin{cases} [M_{\Omega\Omega}] \bar{\mathbf{y}}_\Omega^\ell = -[M_{\Omega\Sigma}] \bar{\mathbf{y}}_\Sigma^\ell, \\ [M_{\Omega\Omega}] \boldsymbol{\varphi}_\Omega^{\ell,j} = -[M_{\Omega\Sigma}] \boldsymbol{\varphi}_\Sigma^{\ell,j}. \end{cases} \quad (4.22)$$

Then, we use polynomial algebra [7, 11, 18] to approximate the product of the jacobian determinant and the inverse of the dilatation tensor involved in (4.7) by a polynomial chaos expansion of order q , written as

$$j(\widehat{\mathbf{Y}}^{\ell,d,h}) [C(\widehat{\mathbf{Y}}^{\ell,d,h})]^{-1} \approx \sum_{|\boldsymbol{\beta}|=0}^q \Gamma_\beta^\ell(\boldsymbol{\eta}^\ell) [G^{\ell,\boldsymbol{\beta}}], \quad (4.23)$$

where $\widehat{\mathbf{Y}}^{\ell,d,h}$ is the FE approximation of the displacement in Ω corresponding to the nodal values $\widehat{\mathbf{Y}}^{\ell,d}$. Finally, we solve a linear problem—inferred from (4.11) by a standard Galerkin projection—that involves finding the coefficients in the polynomial chaos expansion of order q of the nodal values of the potential such that

$$\sum_{|\boldsymbol{\alpha}|=0}^q \sum_{|\boldsymbol{\beta}|=0}^q c_{\boldsymbol{\alpha}\boldsymbol{\beta}\boldsymbol{\gamma}}^\ell [K_{\Omega\Omega}^{\ell,\boldsymbol{\alpha}}] \widehat{\boldsymbol{\phi}}_\Omega^{\ell,\boldsymbol{\beta}} = -[K_{\Omega\Sigma}^{\ell,\boldsymbol{\gamma}}] \boldsymbol{\phi}_\Sigma, \quad 0 \leq |\boldsymbol{\gamma}| \leq q, \quad (4.24)$$

where for $0 \leq |\boldsymbol{\beta}| \leq q$, the matrices $[K^{\ell,\boldsymbol{\beta}}]$ are the FE approximations of the differential operators $\text{div}_{\mathbf{x}}([G^{\ell,\boldsymbol{\beta}}] \nabla_{\mathbf{x}} \cdot)$. The solution of (4.24) provides the following global approximation of the nodal values of the potential:

$$\widehat{\boldsymbol{\Phi}}^{\ell,d,q} = \sum_{|\boldsymbol{\beta}|=0}^q \Gamma_\beta^\ell(\boldsymbol{\eta}^\ell) \widehat{\boldsymbol{\phi}}^{\ell,\boldsymbol{\beta}}, \quad (4.25)$$

and this global approximation immediately provides an approximation in terms of samples by setting $\widehat{\boldsymbol{\Phi}}^\ell(\theta_k) \equiv \widehat{\boldsymbol{\Phi}}^{\ell,d,q}(\theta_k)$, that is,

$$\widehat{\boldsymbol{\Phi}}^\ell(\theta_k) = \sum_{|\boldsymbol{\beta}|=0}^q \Gamma_\beta^\ell(\boldsymbol{\eta}^\ell(\theta_k)) \widehat{\boldsymbol{\phi}}^{\ell,\boldsymbol{\beta}}, \quad 1 \leq k \leq \nu. \quad (4.26)$$

4.9. Selection of dimension d and order q . At each iteration, we select the dimension d as the smallest value that satisfies

$$\sqrt{\frac{1}{\nu} \sum_{k=1}^{\nu} \left\| \widehat{\mathbf{Y}}_\Sigma^\ell(\theta_k) - \widehat{\mathbf{Y}}_\Sigma^{\ell,d}(\theta_k) \right\|^2} \leq \epsilon_1 \sqrt{\frac{1}{\nu} \sum_{k=1}^{\nu} \left\| \widehat{\mathbf{Y}}_\Sigma^\ell(\theta_k) \right\|^2}, \quad (4.27)$$

where ϵ_1 is a prescribed tolerance level. Further, at each iteration, we select the order q as the smallest value that satisfies

$$\sqrt{\frac{1}{\nu} \sum_{k=1}^{\nu} \left\| \widehat{\boldsymbol{\Phi}}^{\ell,d,q}(\theta_k) - \widehat{\boldsymbol{\Phi}}^{\ell,d,q-1}(\theta_k) \right\|^2} \leq \epsilon_2 \sqrt{\frac{1}{\nu} \sum_{k=1}^{\nu} \left\| \widehat{\boldsymbol{\Phi}}^{\ell,d,q}(\theta_k) \right\|^2}, \quad (4.28)$$

where ϵ_2 is a prescribed tolerance level.

4.10. Concluding remarks. Algorithm 1 summarizes the implementation of the stochastic coupled problem by using the proposed hybrid method.

<p>Input : Error tolerance levels ϵ_1 and ϵ_2; Ensemble of samples $\{(\boldsymbol{\xi}(\theta_k), \zeta(\theta_k)), 1 \leq k \leq \nu\}$; $\ell = 0$; repeat $\ell = \ell + 1$; elasticity subproblem for $k = 1$ to ν do Solve $[Z(\widehat{\mathbf{U}}^{\ell-1}(\theta_k), \boldsymbol{\xi}(\theta_k))](\widehat{\mathbf{U}}^\ell(\theta_k) - \widehat{\mathbf{U}}^{\ell-1}(\theta_k)) = -\mathbf{f}(\widehat{\mathbf{U}}^{\ell-1}(\theta_k), \widehat{\mathbf{T}}^{\ell-1}(\theta_k), \boldsymbol{\xi}(\theta_k))$; end Compute $\{\widehat{\mathbf{Y}}_\Sigma^\ell(\theta_k), 1 \leq k \leq \nu\}$ using $\widehat{\mathbf{Y}}_\Sigma^\ell(\theta_k) = \mathbf{h}(\widehat{\mathbf{U}}^\ell(\theta_k))$; end dimension reduction Compute $\bar{\mathbf{y}}_\Sigma^\ell = \frac{1}{\nu} \sum_{k=1}^{\nu} \widehat{\mathbf{Y}}_\Sigma^\ell(\theta_k)$; Compute $[\widehat{\mathbf{C}}_{\mathbf{Y}_\Sigma}^\ell] = \frac{1}{\nu} \sum_{k=1}^{\nu} (\widehat{\mathbf{Y}}_\Sigma^\ell(\theta_k) - \bar{\mathbf{y}}_\Sigma^\ell)(\widehat{\mathbf{Y}}_\Sigma^\ell(\theta_k) - \bar{\mathbf{y}}_\Sigma^\ell)^\top$; Solve $[W^\top \widehat{\mathbf{C}}_{\mathbf{Y}_\Sigma}^\ell W] \boldsymbol{\varphi}_\Sigma^{\ell,j} = \lambda_j^\ell [W] \boldsymbol{\varphi}_\Sigma^{\ell,j}$; Select d such that $\sqrt{\frac{1}{\nu} \sum_{k=1}^{\nu} \ \widehat{\mathbf{Y}}_\Sigma^\ell(\theta_k) - \widehat{\mathbf{Y}}_\Sigma^{\ell,d}(\theta_k)\ ^2} \leq \epsilon_1 \sqrt{\frac{1}{\nu} \sum_{k=1}^{\nu} \ \widehat{\mathbf{Y}}_\Sigma^\ell(\theta_k)\ ^2}$; Compute $\{\boldsymbol{\eta}^\ell(\theta_k), 1 \leq k \leq \nu\}$ using $\boldsymbol{\eta}_j^\ell(\theta_k) = (\widehat{\mathbf{Y}}_\Sigma^\ell(\theta_k) - \bar{\mathbf{y}}_\Sigma^\ell)^\top [W] \boldsymbol{\varphi}_\Sigma^{\ell,j} / \sqrt{\lambda_j^\ell}$; end electrostatics subproblem $q = 0$; repeat $q = q + 1$; Compute $\{\Gamma_\beta^\ell, 0 \leq \beta \leq q\}$ and $\{c_{\alpha\beta\gamma}^\ell, 0 \leq \alpha , \beta , \gamma \leq q\}$; Compute $\bar{\mathbf{y}}^\ell$ and $\{\boldsymbol{\varphi}^{\ell,j}, 1 \leq j \leq d\}$ and assemble $\{[K^{\ell,\beta}], 0 \leq \beta \leq q\}$; Solve $\sum_{ \alpha , \beta =0}^q c_{\alpha\beta\gamma}^\ell [K_{\Omega\Omega}^{\ell,\alpha}] \widehat{\boldsymbol{\phi}}_\Omega^{\ell,\beta} = -[K_{\Omega\Sigma}^{\ell,\gamma}] \boldsymbol{\phi}_\Sigma, 0 \leq \gamma \leq q$; until $\sqrt{\frac{1}{\nu} \sum_{k=1}^{\nu} \ \widehat{\boldsymbol{\Phi}}^{\ell,d,q}(\theta_k) - \widehat{\boldsymbol{\Phi}}^{\ell,d,q-1}(\theta_k)\ ^2} \leq \epsilon_2 \sqrt{\frac{1}{\nu} \sum_{k=1}^{\nu} \ \widehat{\boldsymbol{\Phi}}^{\ell,d,q}(\theta_k)\ ^2}$; Compute $\{\widehat{\mathbf{T}}^\ell(\theta_k), 1 \leq k \leq \nu\}$ with $\widehat{\mathbf{T}}^\ell(\theta_k) = \mathbf{k}(\widehat{\mathbf{Y}}^{\ell,d}(\theta_k), \widehat{\boldsymbol{\Phi}}^{\ell,d,q}(\theta_k), \zeta(\theta_k))$; end until (convergence) ;</p>

Algorithm 1: Implementation of the illustration problem.

Algorithm 1 can be expected to be well adapted to solving the stochastic coupled problem when the random Young modulus field or the random Poisson coefficient field or both have a very high dimension, that is, m_E or m_ν or both are very large, and the KL decomposition is able to accurately characterize the displacement on Σ by a representation of low or moderate dimension d ; here, the displacement on Σ can be expected to admit a representation of low or moderate dimension because it is obtained by solving a stochastic elliptic boundary value problem whose solution can be expected to be smoother than its coefficients because of homogenization associated with its elliptic nature. Indeed, then, Algorithm 1 can be expected to be able to combine the computational efficiency of the Monte Carlo sampling method for solving the elasticity subproblem of “very high dimension” with the computational efficiency of spectral methods for solving the electrostatics subproblem of “low or moderate dimension,” thus making the proposed hybrid method computationally efficient.

5. Numerical results.

5.1. Parameter values. With reference to the Cartesian reference frame (x_1, x_2) with origin \mathbf{o} defined in Fig. 4.1, in the original configuration, we assumed the microbridge to occupy the rectangular region $\mathcal{D} = \{20 \mu\text{m} < x_1 < 120 \mu\text{m}, 4 \mu\text{m} < x_2 < 4.5 \mu\text{m}\}$ and the exterior domain surrounding the microbridge to occupy the region $\Omega = \{0 < x_1 < 140 \mu\text{m}, 0 < x_2 < 50 \mu\text{m}\} \setminus \mathcal{D}$. Thus, in the original configuration, we assumed the microbridge to have a length of $100 \mu\text{m}$, to have a height of $0.5 \mu\text{m}$, and to be separated from the lower horizontal edge of the electrode by a gap of $4 \mu\text{m}$. We assumed a potential difference ϕ^{ext} of 50 V between the microbridge and the electrode. This potential difference was sufficiently large to require that the geometrical coupling of the elastic and electrostatic behavior and the geometrical nonlinearity in the elastic behavior be taken into account, as the results to follow will indicate.

We used a structured mesh of $2400 = 600 \times 4$ four-node quadrilateral elements for the domain occupied by the microbridge and an unstructured mesh of 3482 three-node triangular elements for the exterior domain surrounding the microbridge.

5.2. Nominal coupled problem. First, we used a deterministic and position-independent Young modulus \bar{E} of 65 MPa , Poisson coefficient $\bar{\nu}$ of 0.23 , and electrical permittivity $\bar{\epsilon}_0$ equal to the electrical permittivity of vacuum. We solved the resulting deterministic coupled problem using the Gauss-Seidel partitioned method.

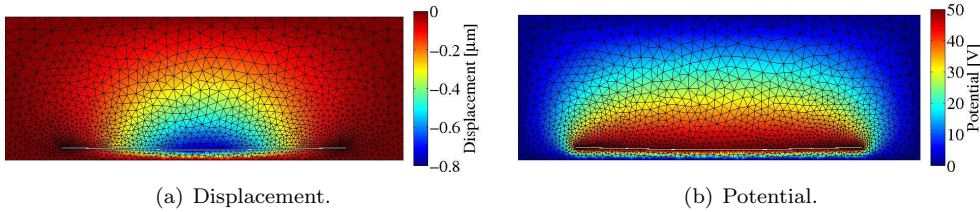


FIG. 5.1. *Nominal coupled problem: (a) displacement and (b) potential.*

Figure 5.1 shows the solution thus obtained. The vertical component of the displacement at the mid point, that is, at $(x_1 = 70 \mu\text{m}, x_2 = 4.25 \mu\text{m})$, was $-0.7582 \mu\text{m}$.

5.3. Stochastic coupled problem. Next, we used random Young modulus and Poisson coefficient fields with position-independent mean values $\bar{E} = 65 \text{ MPa}$ and $\bar{\nu} = 0.23$, spatial correlation lengths $a_E = a_\nu = 5 \mu\text{m}$, and coefficients of variation $\delta_E = \delta_\nu = 2.5\%$, and we used a random electrical permittivity with a mean value equal to the electrical permittivity of vacuum and coefficient of variation $\delta_{\epsilon_0} = 2.5\%$.

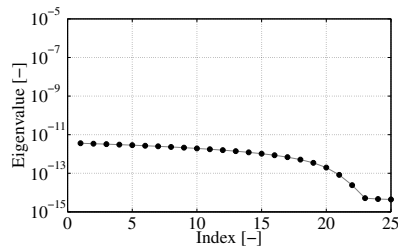


FIG. 5.2. *Stochastic coupled problem: twenty-five largest eigenvalues of the covariance operators whose kernels are given by (4.4) and (4.5).*

Figure 5.2 shows the twenty-five largest eigenvalues of the covariance integral operators whose kernels are given by (4.4) and (4.5). We note that we use the notation $[-]$ in axes labels to indicate dimensionless quantities. We retained $m_E = m_\nu = 25$ terms in (4.1) and (4.2), the adequacy of this truncation being indicated by the decay of the eigenvalues. The modeling of the Young modulus and Poisson coefficient by random fields of dimension $m_E = m_\nu = 25$ and of the electrical permittivity by a random variable results in a stochastic coupled problem of dimension $51 = 25 + 25 + 1$.



FIG. 5.3. Stochastic coupled problem: a few samples of (a) the random Young modulus field and (b) the random Poisson coefficient field as a function of the horizontal position, that is, as a function of x_1 , at the vertical position of the neutral fiber, that is, at $x_2 = 4.25 \mu\text{m}$.

Figures 5.3(a) and 5.3(b) show a few samples of the random fields thus obtained.

5.4. Hybrid method. We implemented the proposed hybrid method as in Algorithm 1. We obtained numerical results using a range of values for the number of samples ν , the number of iterations, and the error tolerance levels ϵ_1 and ϵ_2 . We discuss the convergence later. For now, we present detailed numerical results obtained for $\epsilon_1 = 2.5 \times 10^{-3}$ and $\epsilon_2 = 1 \times 10^{-8}$, for 25 iterations, and for $\nu = 10,000$ samples.

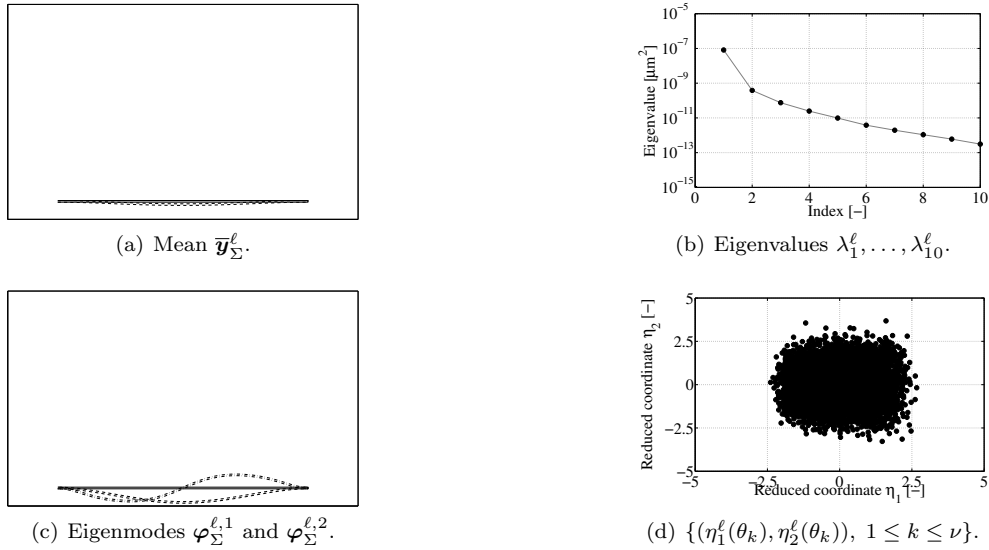


FIG. 5.4. Hybrid method: (a) mean $\bar{\mathbf{y}}_\Sigma^\ell$ (dashed), (b) eigenvalues $\lambda_1^\ell, \dots, \lambda_{10}^\ell$, (c) eigenmodes $\varphi_\Sigma^{\ell,1}$ and $\varphi_\Sigma^{\ell,2}$ (dashed and dash-dotted, respectively; rescaled for clarity), and (d) ensemble of samples $\{(\eta_1^\ell(\theta_k), \eta_2^\ell(\theta_k)), 1 \leq k \leq \nu\}$ of the KL decomposition of $\widehat{\mathbf{Y}}_\Sigma^\ell$ at iteration $\ell = 25$.

Figure 5.4 shows a few components of the KL decomposition of the displacement on Σ obtained at iteration $\ell = 25$. We observe that the eigenvalues of the KL decomposition of the displacement on Σ (Fig. 5.4(b)) decay at a higher rate than those of the KL decompositions that determine the random Young modulus and Poisson coefficient fields (Fig. 5.2). This result is consistent with our earlier observation that the elasticity subproblem can be expected to provide a solution that is smoother than its coefficients owing to its elliptic nature; refer to Sec. 4.10. Further, the high rate of decay of the eigenvalues indicates that the KL decomposition of the displacement on Σ can be truncated after only a small number of terms while accuracy is maintained.

We found that a truncated KL decomposition retaining $d = 2$ terms was sufficiently accurate to satisfy (4.27) for $\epsilon_1 = 2.5 \times 10^{-3}$ at iteration $\ell = 25$. Thus, for this error tolerance level, at this iteration, and in the context of the proposed hybrid method, the elasticity subproblem had a “very high dimension” of $51 = 25 + 25 + 1$ and the electrostatics subproblem had a “low or moderate dimension” of $3 = 2 + 1$.

Because $d = 2$ was sufficiently accurate to satisfy (4.27) for $\epsilon_1 = 2.5 \times 10^{-3}$ at iteration $\ell = 25$, the proposed hybrid method necessitated for this tolerance level at this iteration the construction of two-dimensional polynomial chaos.

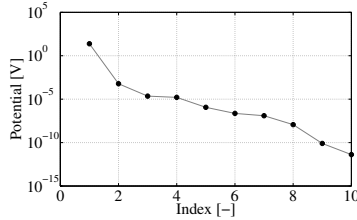


FIG. 5.5. Hybrid method: coefficients in the polynomial chaos expansion of the potential at the point ($x_1 = 70.3392 \mu\text{m}$, $x_2 = 1.9165 \mu\text{m}$) at iteration $\ell = 25$.

We found that a polynomial chaos expansion truncated at order $q = 3$ was sufficiently accurate to satisfy (4.28) for $\epsilon_2 = 1 \times 10^{-8}$ at iteration $\ell = 25$. Figure 5.5 shows a few coefficients involved in the polynomial chaos expansion of the potential obtained for this error tolerance level at this iteration. We observe that the magnitude of the coefficients decreases at a high rate with increasing order.

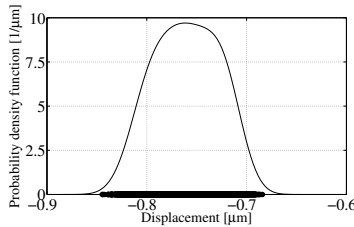


FIG. 5.6. Hybrid method: probability density function of the vertical component of the displacement at the mid point ($x_1 = 70 \mu\text{m}$, $x_2 = 4.25 \mu\text{m}$) at iteration $\ell = 25$.

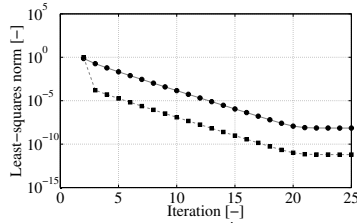
Figure 5.6 shows the probability density function estimated using the kernel density estimation method [14] from the ensemble of samples of the vertical component of the displacement at the mid point obtained at iteration $\ell = 25$. At this iteration, the ensemble of samples of the vertical component of the displacement at the mid point had a sample mean of $-7.600 \times 10^{-1} \mu\text{m}$ and coefficient of variation of 4.199%.

5.5. Convergence study. We conducted the following convergence study to examine the impact of the error tolerance levels ϵ_1 and ϵ_2 , the number of iterations, and the number of samples ν on the numerical results.



FIG. 5.7. *Convergence study: (a) dimension d for $\epsilon_1 = 5 \times 10^{-3}$ (circles), $\epsilon_1 = 2.5 \times 10^{-3}$ (squares), and $\epsilon_1 = 1.25 \times 10^{-3}$ (diamonds) and $\epsilon_2 = 1 \times 10^{-8}$ and (b) order q for $\epsilon_1 = 2.5 \times 10^{-3}$ and $\epsilon_2 = 1 \times 10^{-4}$ (circles), $\epsilon_2 = 1 \times 10^{-6}$ (squares), and $\epsilon_2 = 1 \times 10^{-8}$ (diamonds), as a function of the iteration, and for $\nu = 10,000$ samples.*

For each number of samples ν that we considered, at each iteration ℓ , we selected d and q as the smallest values that satisfy (4.27) and (4.28) for given values of ϵ_1 and ϵ_2 . We ran the proposed hybrid method for several values of ϵ_1 and ϵ_2 . Figures 5.7((a) and (b)) show the values of d and q that were selected as a function of the iteration for $\nu = 10,000$ samples. We observe that a higher dimension and order were selected when we set ϵ_1 and ϵ_2 to lower values and we therefore required higher accuracy.



$$\ell \mapsto \sqrt{\frac{1}{\nu} \sum_{k=1}^{\nu} \|\widehat{\mathbf{U}}^{\ell}(\theta_k) - \widehat{\mathbf{U}}^{\ell-1}(\theta_k)\|^2} \Big/ \sqrt{\frac{1}{\nu} \sum_{k=1}^{\nu} \|\widehat{\mathbf{U}}^{\infty}(\theta_k)\|^2} \text{ (circles).}$$

$$\ell \mapsto \sqrt{\frac{1}{\nu} \sum_{k=1}^{\nu} \|\widehat{\Phi}^{\ell}(\theta_k) - \widehat{\Phi}^{\ell-1}(\theta_k)\|^2} \Big/ \sqrt{\frac{1}{\nu} \sum_{k=1}^{\nu} \|\widehat{\Phi}^{\infty}(\theta_k)\|^2} \text{ (squares).}$$

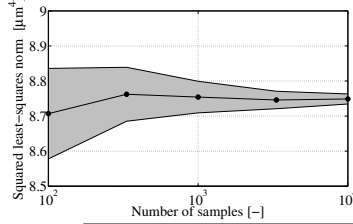
FIG. 5.8. *Convergence study: convergence of the ensembles of samples of the displacement and potential for $\epsilon_1 = 2.5 \times 10^{-3}$ and $\epsilon_2 = 1 \times 10^{-8}$, with respect to the number of iterations, and for $\nu = 10,000$ samples.*

For each number of samples ν that we considered, and while selecting d and q at each iteration as mentioned previously, we monitored the convergence of the ensembles of samples of the displacement in \mathcal{D} and potential with respect to the number of iterations. Figure 5.8 shows the convergence of these ensembles of samples for $\epsilon_1 = 2.5 \times 10^{-3}$ and $\epsilon_2 = 1 \times 10^{-8}$, with respect to the number of iterations, and for $\nu = 10,000$ samples; we note that we use the superscript ∞ in figure captions to indicate results that have converged with respect to the number of iterations. We observe linear convergence up to iteration $\ell = 20$, after which the effects of rounding errors due to the machine precision became significant and prevented further convergence.



FIG. 5.9. *Convergence study: (a) sample average (circles) and 95% confidence region for the mean (filled) and (b) sample variance (circles) and 95% confidence region for the variance (filled) of the vertical component of the displacement at the mid point ($x_1 = 70 \mu\text{m}$, $x_2 = 4.25 \mu\text{m}$) for $\epsilon_1 = 2.5 \times 10^{-3}$ and $\epsilon_2 = 1 \times 10^{-8}$ as a function of the number of samples.*

While selecting the number of iterations sufficiently high for the effects of rounding errors to prevent further convergence and while selecting d and q at each iteration as mentioned previously, we monitored the convergence of estimates of statistical descriptors of the displacement in \mathcal{D} and potential with respect to the number of samples. Figure 5.9 shows the convergence of estimates obtained for the mean and variance of the vertical component of the displacement at the mid point using $\epsilon_1 = 2.5 \times 10^{-3}$ and $\epsilon_2 = 1 \times 10^{-8}$ with respect to the number of samples. The estimates of the mean and variance obtained for $\epsilon_1 = 2.5 \times 10^{-3}$ and $\epsilon_2 = 1 \times 10^{-8}$ and $\nu = 10,000$ samples were $(-7.600 \pm 0.006) \times 10^{-1} \mu\text{m}$ and $(1.019 \pm 0.020) \times 10^{-3} \mu\text{m}^2$, respectively.



$$\nu \mapsto \left(\frac{1}{\nu} \sum_{k=1}^{\nu} \|\widehat{\mathcal{U}}^{\infty}(\theta_k)\|^2 \right) \pm 1.96 \sqrt{\left(\frac{1}{\nu} \sum_{k=1}^{\nu} \|\widehat{\mathcal{U}}^{\infty}(\theta_k)\|^4 \right) - \left(\frac{1}{\nu} \sum_{k=1}^{\nu} \|\widehat{\mathcal{U}}^{\infty}(\theta_k)\|^2 \right)^2} / \sqrt{\nu}.$$

FIG. 5.10. *Convergence study: square of the least-squares norm (circles) and 95% confidence region for the square of the least-squares norm (filled) of the displacement in \mathcal{D} for $\epsilon_1 = 2.5 \times 10^{-3}$ and $\epsilon_2 = 1 \times 10^{-8}$ as a function of the number of samples.*

Similarly, Fig. 5.10 shows the convergence of an estimate obtained for the square of the least-squares norm of the displacement in \mathcal{D} using $\epsilon_1 = 2.5 \times 10^{-3}$ and $\epsilon_2 = 1 \times 10^{-8}$ with respect to the number of samples. The estimate obtained using $\epsilon_1 = 2.5 \times 10^{-3}$ and $\epsilon_2 = 1 \times 10^{-8}$ and $\nu = 10,000$ samples was equal to $(8.748 \pm 0.014) \mu\text{m}^4$.

5.6. Comparison with Monte Carlo sampling method. We also implemented the Gauss-Seidel partitioned method in (4.10)–(4.11) using solely the Monte Carlo sampling method as in Sec. 2.3. We used as the ensemble of i.i.d. samples $\{(\xi(\theta_k), \zeta(\theta_k)), 1 \leq k \leq \nu\}$ for the implementation that uses solely the Monte Carlo sampling method precisely the ensemble that we had used before for the implementation that uses the proposed hybrid method, thus enabling direct comparison of the samples of the displacement in \mathcal{D} and potential provided by these implementations.

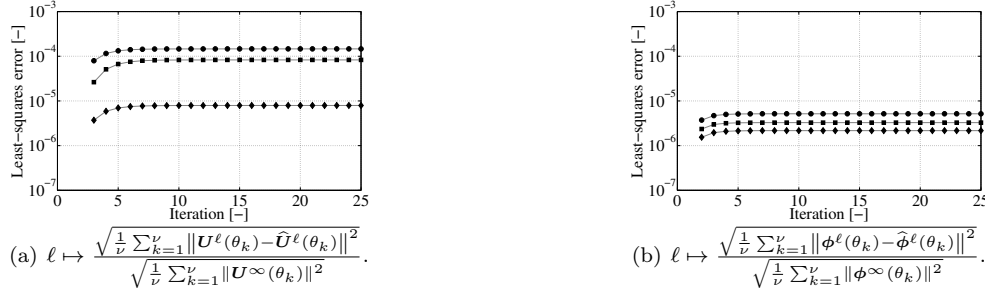


FIG. 5.11. Comparison with Monte Carlo sampling method: least-squares norm of the difference of the displacement in \mathcal{D} and potential provided by the Monte Carlo sampling and the proposed hybrid method for $\epsilon_1 = 5 \times 10^{-3}$ (circles), $\epsilon_1 = 2.5 \times 10^{-3}$ (squares), and $\epsilon_1 = 1.25 \times 10^{-3}$ (diamonds) and $\epsilon_2 = 1 \times 10^{-8}$, as a function of the iteration, and for $\nu = 10,000$.

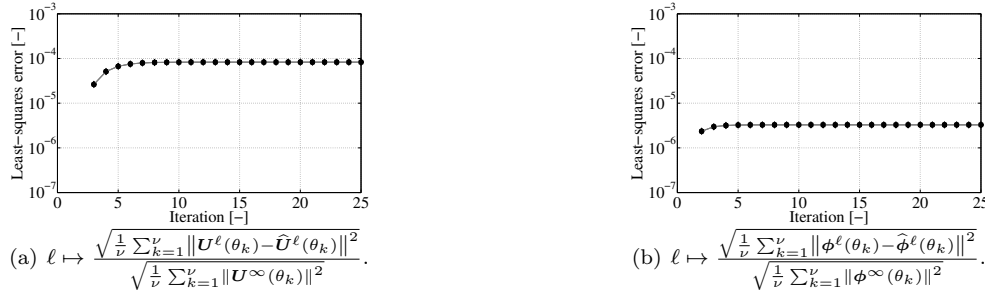


FIG. 5.12. Comparison with Monte Carlo sampling method: least-squares norm of the difference of the displacement in \mathcal{D} and potential provided by the Monte Carlo sampling and the proposed hybrid method for $\epsilon_1 = 2.5 \times 10^{-3}$ and $\epsilon_2 = 1 \times 10^{-4}$ (circles), $\epsilon_2 = 1 \times 10^{-6}$ (squares), and $\epsilon_2 = 1 \times 10^{-8}$ (diamonds), as a function of the iteration, and for $\nu = 10,000$.

Figures 5.11 and 5.12 compare the numerical results provided by the implementation that uses solely the Monte Carlo sampling method with those provided by the implementation that uses the proposed hybrid method. We observe that the difference between the samples of the displacement in \mathcal{D} and potential provided by these implementations remained bounded as the iterations progressed and was reduced systematically when we improved the accuracy of the KL decomposition of the displacement on Σ and the polynomial chaos expansion of the potential by decreasing ϵ_1 and ϵ_2 .

The estimates for the mean and variance of the vertical component of the displacement at the mid point and that for the square of the least-squares norm of the displacement in \mathcal{D} provided by the implementation that uses solely the Monte Carlo sampling method were equal to $(-7.600 \pm 0.006) \times 10^{-1} \mu\text{m}$, $(1.019 \pm 0.020) \times 10^{-3} \mu\text{m}^2$, and $(8.748 \pm 0.014) \mu\text{m}^4$, respectively. They are identical to those given in the previous section for the implementation that uses the proposed hybrid method for $\epsilon_1 = 2.5 \times 10^{-3}$ and $\epsilon_2 = 1 \times 10^{-8}$. Hence, at least for these values of the error tolerance levels, the truncation error—which may exist in the estimates provided by the implementation that uses the proposed hybrid method owing to the solution of the electrostatics subproblem by a spectral method in only a reduced-dimensional space for only a truncated polynomial chaos expansion; refer to Sec. 2.6—is dominated by the sampling error because it leaves unaffected all significant digits.

5.7. Effectiveness. We assessed the computational efficiency of the proposed hybrid method for solving the illustration problem described previously as follows.

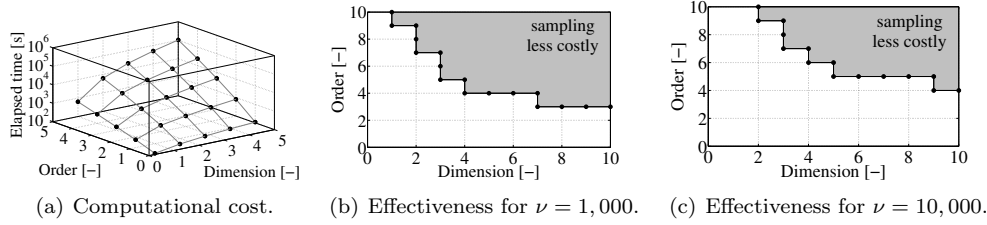


FIG. 5.13. *Effectiveness: (a) time required for solving the elasticity subproblem using a spectral method as a function of the dimension of this subproblem, that is, $m_E + m_\nu + 1$, and the order of the sought polynomial chaos expansion of the displacement in \mathcal{D} and (b,c) values of the dimension and order for which this time is larger than that required for solving the elasticity subproblem using the Monte Carlo sampling method with either $\nu = 1,000$ or $\nu = 10,000$ samples.*

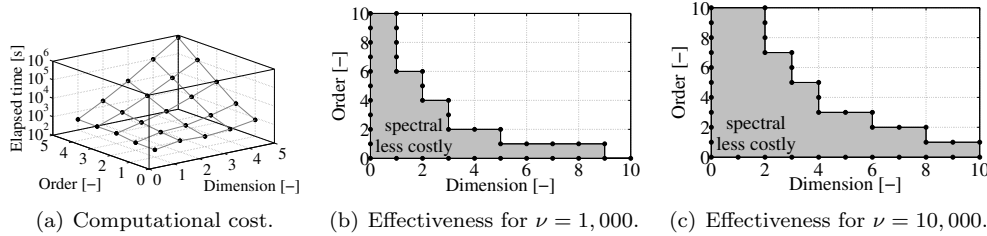


FIG. 5.14. *Effectiveness: (a) time required for solving the electrostatics subproblem using a spectral method as a function of the dimension of this subproblem, that is, $d + 1$, and the order of the sought polynomial chaos expansion of the potential and (b,c) values of the dimension and order for which this time is smaller than that required for solving the electrostatics subproblem using the Monte Carlo sampling method with either $\nu = 1,000$ or $\nu = 10,000$ samples.*

For several combinations of values of m_E , m_ν , d , q , and ν , we repeated the following study. For each combination of values of m_E , m_ν , d , q , and ν , first, we solved the coupled elasticity/electrostatics problem using the proposed hybrid method. Once convergence with respect to the number of iterations was obtained, we halted the proposed hybrid method and then focused our attention on the elasticity and electrostatics subproblems that were solved at the last iteration: For this elasticity subproblem, we compared the time that a single-core computer required to obtain the solution using a spectral method with the time that this single-core computer required to obtain the solution using the Monte Carlo sampling method; likewise, for this electrostatics subproblem, we compared the time that a single-core computer required to obtain the solution using a spectral method with the time that this single-core computer required to obtain the solution using the Monte Carlo sampling method.

Figures 5.13 and 5.14 summarize our findings. On the one hand, the time required by the spectral method to obtain the solution to the elasticity subproblem increased quickly with its dimension and with the order of the polynomial chaos expansion of the displacement in \mathcal{D} but was essentially independent of the number of samples (Fig. 5.13(a)); likewise, the time required by the spectral method to obtain the solution to the electrostatics subproblem increased quickly with its dimension and

with the order of the polynomial chaos expansion of the potential but was essentially independent of the number of samples (Fig. 5.14(a)). On the other hand, the time required by the Monte Carlo sampling method to obtain the solution increased proportionally to the number of samples. Correspondingly, for both the elasticity and the electrostatics subproblem, we can observe that the set of combinations of values of the dimension and order for which the spectral method required less time than the Monte Carlo sampling method was limited to low and moderate values of the dimension and order and reached to higher values of the dimension and order when we increased the number of samples (Figs. 5.13((b) and (c)) and 5.14((b) and (c))).

We emphasize that the distinction between subproblems of “very high dimension” and those of “low or moderate dimension” in Figs. 5.13 and 5.14 applies only to our implementation of the coupled elasticity/electrostatics problem under study: whether values of the dimension and order are very high or low or moderate depends on the problem specificities and solver technology used, as well as on the number of samples.

We conclude that the proposed hybrid method is computationally efficient for solving the illustration problem described previously in Secs. 5.1–5.6. Indeed, while the elasticity subproblem was of “very high dimension” because we represented the elastic coefficients by high-dimensional random fields (Sec. 5.3), the proposed hybrid method allowed the electrostatics subproblem to be solved in a low-dimensional space because the KL decomposition was able to extract a low-dimensional representation of the displacement on Σ (Secs. 5.4 and 5.5), while maintaining accuracy (Sec. 5.6). Accordingly, the proposed hybrid method was computationally efficient for solving the illustration problem because it allowed the computational efficiency of the Monte Carlo sampling method for solving the elasticity subproblem of “very high dimension” to be combined with the computational efficiency of a spectral method for solving the electrostatics subproblem of “low or moderate dimension” (Figs. 5.13 and 5.14).

6. Conclusion. We proposed a hybrid Monte Carlo sampling/spectral method for solving stochastic coupled problems. The main feature of the proposed hybrid method is that it allows uncertainties to be accurately propagated through coupled problems and yet can be implemented as a wrapper around separate methods for the propagation of uncertainties through subproblems, where the most computationally efficient Monte Carlo sampling or spectral method can be used. After laying out the theoretical framework, we demonstrated the proposed hybrid method by applying it to a stochastic multiphysics problem relevant to microelectromechanical systems.

In the illustration problem, we studied some issues relevant to error analysis, stability, and convergence from a numerical point of view. The complementary study of such issues from a theoretical point of view using, for example, *a posteriori* error estimation methods [4], constitutes an interesting direction for future work.

Acknowledgments. The authors would like to thank the two anonymous reviewers for their thoughtful suggestions.

References.

- [1] M. ARNST, R. GHANEM, E. PHIPPS, AND J. RED-HORSE, *Dimension reduction in stochastic modeling of coupled problems*, International Journal for Numerical Methods in Engineering, 92 (2012), pp. 940–968. DOI: 10.1002/nme.4364.
- [2] ———, *Measure transformation and efficient quadrature in reduced-dimensional stochastic modeling of coupled problems*, International Journal for Numerical Methods in Engineering, 92 (2012), pp. 1044–1080. DOI: 10.1002/nme.4368.

- [3] T. BELYTSCHKO, W. LIU, AND B. MORAN, *Nonlinear Finite Elements for Continua and Structures*, John Wiley & Sons, Chichester, United Kingdom, 2000.
- [4] V. CAREY, D. ESTEP, AND S. TAVENER, *A posteriori analysis and adaptive error control for multiscale operator decomposition solution of elliptic systems I: Triangular systems*, SIAM Journal on Numerical Analysis, 47 (2008), pp. 740–761. DOI: 10.1137/070689917.
- [5] A. DOOSTAN AND G. IACCARINO, *A least-squares approximation of partial differential equations with high-dimensional random inputs*, Journal of Computational Physics, 228 (2009), pp. 4332–4345. DOI: 10.1016/j.jcp.2009.03.006.
- [6] M. ESPIG, W. HACKBUSCH, A. LITVINENKO, H. MATTHIES, AND P. WÄHNERT, *Efficient low-rank approximation of the stochastic Galerkin matrix in tensor formats*, Computers and Mathematics with Applications, (2012). DOI: 10.1016/j.camwa.2012.10.008.
- [7] R. GHANEM AND P. SPANOS, *Stochastic Finite Elements: A Spectral Approach*, Dover Publications, Mineola, New York, 2003.
- [8] G. GOLUB AND G. MEURANT, *Matrices, Moments and Quadrature with Applications*, Princeton University Press, Princeton, New Jersey, 2009.
- [9] G. GOLUB AND C. VAN LOAN, *Matrix computations*, The Johns Hopkins University Press, Baltimore, Maryland, 1996.
- [10] J. GUILLEMINOT AND C. SOIZE, *On the statistical dependence for the components of random elasticity tensors exhibiting material symmetry properties*, Journal of Elasticity, 34 (2012), pp. A2917–A2945. DOI: 10.1007/s10659-012-9396-z.
- [11] O. LE MAÎTRE AND O. KNIO, *Spectral Methods for Uncertainty Quantification: With Applications to Computational Fluid Dynamics*, Springer, New York, 2010.
- [12] G. PERRIN, C. SOIZE, D. DUHAMEL, AND C. FUNFSCHILLING, *Identification of polynomial chaos representations in high dimension from a set of realizations*, SIAM Journal on Scientific Computing, 34 (2012), pp. A2917–A2945. DOI: 10.1137/11084950X.
- [13] C. ROBERT AND G. CASELLA, *Monte Carlo Statistical Methods*, Springer, New York, 2010.
- [14] D. SCOTT, *Multivariate Density Estimation: Theory, Practice, and Visualization*, Wiley, New York, 1992.
- [15] C. SOIZE, *Identification of high-dimension polynomial chaos expansions with random coefficients for non-Gaussian tensor-valued random fields using partial and limited experimental data*, Computer Methods in Applied Mechanics and Engineering, 199 (2010), pp. 2150–2164. DOI: 10.1016/j.cma.2010.03.013.
- [16] ———, *A computational inverse method for identification of non-Gaussian random fields using the Bayesian approach in very high dimension*, Computer Methods in Applied Mechanics and Engineering, 200 (2011), pp. 3083–3099. DOI: 10.1016/j.cma.2011.07.005.
- [17] C. SOIZE AND C. DESCIELIERS, *Computational aspects for constructing realizations of polynomial chaos in high dimension*, SIAM Journal on Scientific Computing, 32 (2010), pp. 2820–2831. DOI: 10.1137/100787830.
- [18] C. SOIZE AND R. GHANEM, *Physical systems with random uncertainties: Chaos representations with arbitrary probability measure*, SIAM Journal on Scientific Computing, 26 (2004), pp. 395–410. DOI: 10.1137/S1064827503424505.
- [19] D. XIU, *Numerical Methods for Stochastic Computations: A Spectral Method Approach*, Princeton University Press, Princeton, New Jersey, 2010.